

1 Biogeochemical and biophysical responses to episodes of wildfire smoke from 2 natural ecosystems in southwestern British Columbia, Canada

3
4 Sung-Ching Lee¹, Sara H. Knox¹, Ian McKendry¹, T. Andrew Black²

5
6 ¹Department of Geography, University of British Columbia, Vancouver, Canada

7 ²Faculty of Land and Food Systems, University of British Columbia, Vancouver,
8 Canada

9
10 **Correspondence:** Sung-Ching Lee (sungching.lee@geog.ubc.ca)

11 **Abstract**

12
13 Area burned, number of fires, seasonal fire severity, and fire season length are all
14 expected to increase in Canada, with largely unquantified ecosystem feedbacks.
15 However, there are few observational studies measuring ~~the~~ ecosystem-scale
16 biogeochemical (e.g., carbon-dioxide exchanges) and biophysical (e.g., energy
17 partitioning) properties during smoke episodes, and hence ~~a~~ ess essing responses of
18 gross primary production (GPP) to changes in incoming productivity effects of
19 changes in incident diffuse photosynthetically active radiation (PAR). In this study,
20 we leverage two long-term eddy-eddy-covariance measurement sites in forest and
21 wetland ecosystems to study four smoke episodes, which happened at different times
22 and differed in length, over four different years (2015, 2017, 2018 and 2020). We
23 found that the highest decrease of shortwave irradiance due to smoke was about 50%
24 in July and August but increased to about 90% when the smoke arrived in September.
25 When the smoke arrived in the later stage of summer, impacts on sensible and latent
26 heat fluxes ~~H and LE~~ were also greatest. Smoke generally increased the diffuse
27 fraction (DF) from ~0.30 to ~0.50 and turned both sites into stronger carbon-dioxide
28 (CO₂) sinks with increased GPP up to productivity of ~18% and ~7% at the forest and
29 wetland sites, respectively. However, when DF ~~the diffuse fraction~~ exceeded 0.80 as a
30 result of dense smoke, both ecosystems became net CO₂ sources as total PAR dropped
31 to low values. The results suggest that this kind of natural experiment is important for
32 validating future predictions of smoke-productivity feedbacks.

33 34 35 **1 Introduction**

36 Among the many ecosystem services provided by temperate forests and wetlands in
37 western North America, climate regulation is identified as one of their most important
38 benefits to society (Millennium Ecosystem Assessment, 2005). However, these

39 services are being greatly altered by increasing wildfire occurrences, both in terms of
40 frequency and duration (Settele et al., 2015). In addition to affecting visibility and air
41 quality, aerosols arising from biomass burning can alter the radiation budget by
42 scattering and absorbing radiation and hence potentially influence cloud processes
43 (Crutzen & Andreae, 1990). The overall effect of aerosols on climate still remains
44 uncertain according to the latest IPCC assessment (Pachauri et al., 2014). This has
45 triggered enormous interest in the radiative impacts of smoke plumes induced by
46 biomass burning (Chubarova et al., 2012; Lasslop et al., 2019; Markowicz et al.,
47 2017; McKendry et al., 2019; Moreira et al., 2017; Oris et al., 2014; Park et al., 2018;
48 Sena et al., 2013). Heavy smoke conditions were found to cause net surface cooling of
49 3 °C in Amazonia (Yu et al., 2002), while some have observed net radiative cooling at
50 the surface and net radiative warming at the top of the atmosphere in the Arctic and
51 southeastern United States (Markowicz et al., 2017; Taubman et al., 2004), resulting
52 in enhanced atmospheric stability. It has been estimated that aerosol emissions from
53 boreal fires might have a net effect of inducing a positive feedback to global warming
54 (Oris et al., 2014). Jacobson (2014) also suggested a net global warming of 0.4 K by
55 including black and brown atmospheric carbon, heat and moisture fluxes, and cloud
56 absorption effects. However, other studies using atmospheric modelling found a net
57 cooling effect of aerosols, which can lead to a net reduction in the global radiative
58 forcing of fires (Landry et al., 2015; Ward et al., 2012).

59 Changes in solar irradiance, in particular photosynthetically active radiation
60 (PAR, 400–700 nm), affect plant physiological mechanisms that influence
61 photosynthesis (i.e., gross primary production (GPP)), net ecosystem exchange of
62 CO₂ (NEE), and light use efficiency (LUE). Sub-canopy leaves, especially in forest
63 ecosystems, typically remain under light-deficit conditions. Increasing diffuse
64 radiation makes it easier for PAR photons to penetrate deeper into the canopy
65 (Doughty et al., 2010; Kanniah et al., 2012; Knohl and Baldocchi, 2008; Rap et al.,
66 2015). Additionally, diffuse PAR coming from different angles can increase the
67 efficiency of CO₂ assimilated by plants because leaves are generally at different
68 orientations (Alton et al., 2006). This increase in photosynthesis that results from the
69 trade-off between decreased solar radiation and increased PAR scattering is referred
70 to as the diffuse radiation fertilization (DRF) effect (Moreira et al., 2017; Park et al.,
71 2018; Rap et al., 2015). However, DRF has not always been observed under fire
72 smoke conditions and appears to be ecosystem-dependent. For instance, Ezhova et al.,
73 (2018) found that the mechanisms causing the increases in GPP are different between
74 the boreal coniferous and mixed forest ecosystems. Some studies suggest that DRF
75 might depend on canopy height and the leaf area index (LAI) (Cheng et al., 2015;
76 Kanniah et al., 2012; Niyogi et al., 2004). For example, Cheng et al. (2015) found an

77 increase in GPP due to diffuse radiation for forest sites but not for cropland sites using
78 AmeriFlux data from ten temperate climate ecosystems including three forests and
79 seven croplands. Therefore, it is still uncertain how ~~the~~ changes in diffuse radiation
80 affect GPP and it is also ~~not~~unclear how large the effect of aerosols is on diffuse
81 radiation.

82 With an area of 95 million hectares (Ministry of Forests, 2003), British Columbia
83 (BC), Canada, is almost double the size of California, USA. Of that area, almost 64%
84 is forested with less than one-third of one percent of BC's forest land harvested
85 annually (Ministry of Forests, Mines and Land, 2010). Wetlands in BC comprise
86 around 5.28 million hectares, or approximately 5% of the land base (Wetland
87 Stewardship Partnership, 2009). Therefore, responses of forests and wetlands to
88 wildfire smoke are very likely to have a significant impact on regional carbon
89 budgets. In western Canada, a previous study found that a short, but severe, wildfire
90 smoke episode in 2015 appreciably changed the energy balance and net CO₂ exchange
91 at wetland and forest sites in southwestern BC (McKendry et al., 2019). Another
92 study investigated 2017 and 2018 smoke events in southwestern BC and found that
93 the aerosols from wildfires suppressed the development of deep mountain convective
94 layers, and hence inhibited vertical mixing, convection and cloud development
95 (Ferrara et al., 2020). It is unclear whether the changes in NEE found by McKendry et
96 al. (2019) were due to changes in GPP or ecosystem respiration (R_e). Furthermore,
97 biogeochemical and biophysical properties of wetland and forest ecosystems might
98 respond differently to smoke events with different intensities and durations.

99 ~~In 2015, 2017, 2018, and 2020, southwestern BC experienced smoke episodes~~
100 ~~that differed in both duration and intensity.~~

101 In this study, we investigate the effect of those fire events on two natural
102 ecosystems in southwestern BC; one is a temperate forest ecosystem (Douglas-fir,
103 *Pseudotsuga menziesii*) and the other is a wetland ecosystem (restored peatland) (Fig.
104 1). We aim to provide a better understand of biogeochemical and biophysical
105 responses to wildfire smoke episodes in natural ecosystems in southwestern BC.
106 Specifically, we aim to (1) evaluate smoke-induced changes in shortwave irradiance,
107 albedo, and energy partitioning at the two sites, (2) assess the biogeochemical
108 responses to smoke by investigating GPP and R_e at the two sites, and (3) estimate the
109 maximum effect of smoke on GPP due to changes in the ratio of diffuse to total PAR.
110 Ultimately, we hope to provide a firm foundation for upscaling the impacts of wildfire
111 smoke on the regional CO₂ budget.

112 **2 Methodology**

113 **2.1 Wildfire smoke episodes**

114 **2.1.1 Overview**

115 In 2015, there were a series of wildfires across different provinces in Canada. During
116 4–8 July 2015, smoke spread across most of North America and a particularly intense
117 event occurring in ~150 km north of Vancouver seriously impacted air quality and
118 visibility in southwestern BC. The detailed evolution and synoptic patterns associated
119 with this event are described in McKendry et al. (2019). In summer 2017, a smoke
120 haze settled over the BC coast due to offshore winds advecting smoke from wildfires
121 in the BC Interior. The wildfire season in 2018 eclipsed the previous year's as the
122 worst recorded in BC history with 2,117 fires consuming 1,354,284 hectares of land.
123 ([https://www2.gov.bc.ca/gov/content/safety/wildfire-status/about-bcws/wildfire-
124 history/wildfire-season-summary](https://www2.gov.bc.ca/gov/content/safety/wildfire-status/about-bcws/wildfire-
124 history/wildfire-season-summary)). Smoke covered the BC coast area for
125 approximately 20 days with additional plumes drifting north from similar fires in
126 Washington state, USA. In 2020, BC recorded a quiet fire season with 637 wildfires
127 burning just over 15,000 hectares of land between 1 April and 1 October. However,
128 southwestern BC was significantly affected by smoke advected northward from an
129 intense fire season affecting Washington state, Oregon, and California, USA. Notably,
130 the cross-border smoke arrived in September, somewhat later than usual.
131



132

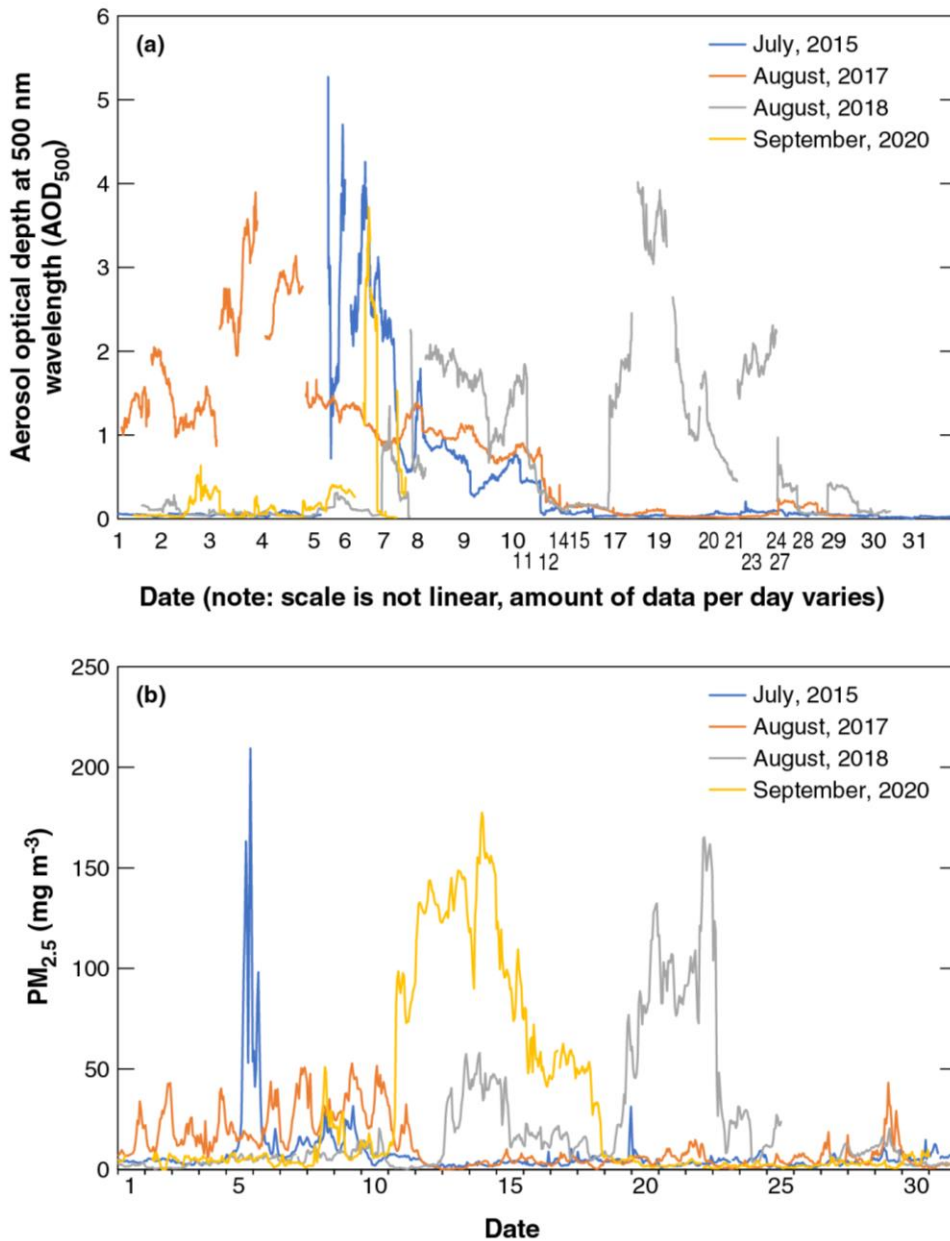
133 **Figure 1.** Locations of the all sites mentioned in text. Observations of aerosol optical
 134 depth at the reference 500 nm wavelength (AOD_{500}) and particulate matter less than
 135 $2.5 \mu\text{m}$ in diameter ($PM_{2.5}$) were collected at Saturna Island AERONET site and
 136 Vancouver International Airport, respectively. Flux and climate data of wetland and
 137 forest ecosystems were measured at Burns Bog and Buckley Bay, respectively.

138 2.1.2 AERONET and AEROCAN

139 The global AERONET (AERosol RObotic NETwork) has been in operation since 1993
140 and is focused on measurements of vertically integrated aerosol properties using the
141 CIMEL sunphotometer/sky radiometer instrument (Holben et al., 1998). AEROCAN
142 CIMELs (AEROCAN is the Canadian sub-network of AERONET) include a facility
143 on Saturna Island, which is located 55 km to the south of the city of Vancouver (Fig.
144 1). Here, solar irradiance is acquired across eight spectral channels (340, 380, 440, 500,
145 670, 870, 1020 and 1640 nm) that are transformed into three processing levels of
146 aerosol optical depth (AOD); 1.0 – non-cloud screened; 1.5 – cloud screened; and 2.0
147 – cloud screened and quality assured. McKendry et al. (2011) demonstrated the
148 application of these data to the transport of California wildfire plumes. In this paper,
149 we present the level 1.5 AOD data at the reference 500 nm wavelength (AOD₅₀₀) in
150 order to compare both the magnitude and duration of the four smoke episodes. The
151 AOD₅₀₀ ranged from 0 to 0.2 on the average cloudless summer days on Saturna Island.

152 The monthly course of AOD₅₀₀ for each of four episodes at Saturna Island is
153 shown in Fig. 2a. Due to technical difficulties, numbers of AOD₅₀₀ data points per day
154 were inconsistent. For each event there were persistent multi-day periods when
155 AOD₅₀₀ > 2 and reached or exceeded a value of 4. The impact of smoke events on
156 ground level PM_{2.5} (particulate matter less than 2.5 µm in diameter) concentrations at
157 Vancouver International Airport is shown in Fig. 2b, and there were 24 PM_{2.5} data
158 points for each day. From Fig. 2, it is evident that the smoke event of 2015, although
159 the shortest of the four events, was the most intense with both AOD₅₀₀ >5 and ground
160 level PM_{2.5} concentrations >200 µg m⁻³, ~~exceeding those of the other three events.~~
161 This is likely due to the close proximity of the fires in this case (McKendry et al.
162 2019). The event of August 2017 was of somewhat longer duration in which AOD₅₀₀
163 peaked at 4 but ground level concentrations remained comparatively low (<50 µg m⁻³)
164 and showed a strong diurnal pattern associated with boundary layer entrainment from
165 elevated layers (Ferrara et al. 2020). In August 2018 the smoke was persistent and
166 included a double maximum. Ground level PM_{2.5} concentrations exceeded 150 µg m⁻³
167 and AOD₅₀₀ reached 4. Finally, the early fall event in September 2020 was also a
168 persistent event in which ground level concentrations exceeded 150 µg m⁻³ and
169 AOD₅₀₀ reached 4. There was evidence in this case of two short peaks in smoke in
170 late September that followed the main event. The impact of smoke events on ground
171 level ozone concentrations (O₃) at Vancouver International Airport and Nanaimo
172 Labieux Road Station on Vancouver Island is shown in Table 1. For all of the study
173 periods, the maximum daily average O₃ was below 25 ppb. The averages of the four
174 months in the four years were ~16 ppb.

175 In summary, the four events were all quite different with respect to intensity of
176 smoke, duration, and impact at ground level (a function of transport height of smoke
177 layers and boundary layer processes). The most similar in character appear to be the
178 2018 and 2020 events, although it is likely that the “age” and life history of smoke
179 was different for these two cases due to the different geographical sources and
180 distances travelled.
181



182
183 **Figure 2. (a)** AOD₅₀₀ at Saturna Island and **(b)** PM_{2.5} observations at Vancouver
184 International Airport for the four months with wildfire smoke in Vancouver, British

185 Columbia, Canada. There are different numbers of AOD₅₀₀ data points per day in
186 panel a and 24 PM_{2.5} data points per day in panel b.
187

188 **2.1.3 Study periods**

189 Study periods were defined using the following criteria. First, days were selected with
 190 $AOD_{500} > 0.5$ or $PM_{2.5} > 50 \mu g m^{-3}$. Second, Hazard Mapping System Fire and Smoke
 191 Product from The Office of Satellite and Product Operations at the National Oceanic
 192 and Atmospheric Administration were used to plot smoke polygons over the region of
 193 southwestern British Columbia region. In the final step, we included a day into the study
 194 periods when the two sites were covered by the smoke polygon classified in the medium
 195 category. The study periods during the four months with wildfire smoke and the
 196 respective maximum AOD₅₀₀, PM_{2.5}, and O₃ values~~AOD₅₀₀ and PM_{2.5}~~ values are
 197 summarized in Table 1. To assess how smoke altered biophysical and biogeochemical
 198 properties under representative environmental conditions in different months, we
 199 compared the study periods with the non-smoky days, which were the remaining days
 200 in the same month.

201

202 **Table 1.** Summaries for the four study periods.

<u>Year</u>	<u>Study period</u>	<u>Maximum</u> <u>AOD₅₀₀</u>	<u>Maximum</u> <u>PM_{2.5} (mg m⁻³)</u>	<u>Daily average O₃</u> <u>(ppb)</u>
<u>2015</u>	<u>4–8 July</u>	<u>5.3</u>	<u>210</u>	<u>24^b, 24^c</u>
<u>2017</u>	<u>1–11 August</u>	<u>3.9</u>	<u>53</u>	<u>15^b, 24^c</u>
<u>2018</u>	<u>8–23 August</u>	<u>4.0</u>	<u>165</u>	<u>15^b, 23^c</u>
<u>2020</u>	<u>8–18 September</u>	<u>3.7^a</u>	<u>178</u>	<u>14^b, 20^c</u>

203 ^aThere were no available observations during the 2020 smoke episode. The value shown
 204 here was observed on 6 September 2020.

205 ^bThe measurements were collected at Vancouver International Airport Station. The
 206 monthly O₃ averages were 20, 16, 15, 15 ppb during July 2015, August 2017, August
 207 2018, September 2020, respectively.

208 ^cThe measurements were collected at Nanaimo Labieux Road Station. The monthly O₃
 209 averages were 20, 22, 21, 18 ppb during July 2015, August 2017, August 2018,
 210 September 2020, respectively.

211 **Table 1.** Summaries for the four study periods.

<u>Year</u>	<u>Study period</u>	<u>Maximum AOD₅₀₀</u>	<u>Maximum PM_{2.5} (μg m⁻³)</u>
<u>2015</u>	<u>4–8 July</u>	<u>5.3</u>	<u>210</u>
<u>2017</u>	<u>1–11 August</u>	<u>3.9</u>	<u>53</u>
<u>2018</u>	<u>8–23 August</u>	<u>4.0</u>	<u>165</u>
<u>2020</u>	<u>8–18 September</u>	<u>3.7[*]</u>	<u>178</u>

212 ^{*}There were no available observations during the 2020 smoke episode. The value
 213 shown here was observed on 6 September 2020.

214

215 2.2 Radiative and turbulent flux measurements

216 2.2.1 Wetland site

217 The rewetted peatland site (AmeriFlux ID: CA-DBB, 122°59'5.60" W, 49°07'45.59"
218 N) (Christen & Knox, 2021) is located in the centre of the Burns Bog Ecological
219 Conservancy Area in British Columbia, Canada (Fig. 1). Burns Bog is recognized as
220 the largest raised bog ecosystem on the west coast of Canada (Christen et al., 2016).
221 The 5-m-tall flux tower at Burns Bog was built in 2014, and is equipped with an eddy
222 covariance (EC) system to continuously measure turbulent fluxes of sensible heat (H),
223 latent heat (LE), and carbon dioxide (F_{CO_2}). F_{CO_2} and the turbulent heat fluxes were
224 computed using the 30-min covariance of turbulent fluctuations in the vertical wind
225 speed and the scalar of interest, and standard quality control ~~involved~~involving
226 removing spikes was applied to half-hourly EC-measured fluxes. We applied block
227 averaging and time-lag removal by covariance maximization (Moncrieff et al., 1997).
228 Coordinate rotations were performed so that mean wind speeds ~~at~~for each 30-min
229 averaging interval were zero in the cross-wind and vertical directions. The flux data
230 were further filtered to exclude the errors indicated by the sonic anemometer and
231 IRGA diagnostic flags, typically attributable to heavy rainfall or snowfall. Fluxes
232 were also filtered for spikes in 30-min mean mixing ratios, variances and covariances
233 with thresholds. F_{CO_2} was corrected by adding the estimated rate of change in CO₂
234 storage in the air column below the EC sensor height to obtain NEE (Hollinger et al.,
235 1994; Morgenstern et al., 2004). After obtaining cleaned heat fluxes, we filtered NEE
236 and heat fluxes ~~with~~for low friction velocity (u_*). The u_* threshold was 0.03 m s⁻¹
237 determined by using the moving point test (Papale et al., 2006). The algorithm used
238 for u_* threshold detection was run in R (R Core Team, 2017) by using the
239 REdyProc 1.2-2 R package (Wutzler et al., 2018). NEE was partitioned into GPP
240 and R_e using a nighttime-based partitioning method (Reichstein et al., 2005). Four
241 components of radiation (shortwave, longwave, incoming, and outgoing) were
242 continuously measured by a four-component net radiometer (CNR1, Kipp and Zonen,
243 Delft, Holland) on the top of the tower. The surface albedo (α) of the site, i.e., the
244 ratio of the reflected shortwave radiation (K_{\uparrow}) to the shortwave irradiance (K_{\downarrow}), was
245 ~~measured~~estimated at noon. Total incoming PAR (PAR_g) was measured using a
246 quantum sensor (LI-190, LI-COR Inc., Lincoln, NE, USA) at the same height. Several
247 climate variables were also measured (e.g., net radiation (R_n), relative humidity (RH),
248 and water table level). Further details of the site are described in Christen et al.
249 (2016), Lee et al. (2017), and D'Acunha et al. (2019).

250

251 2.2.2 Forest site

252 Buckley Bay (AmeriFlux ID: CA-Ca3) is a flux tower with EC and radiation sensors
253 measuring exchanges between a coniferous forest stand (Douglas-fir, 27 years old)
254 and the atmosphere (Black, 2021). The site is located on the eastern slopes of the
255 Vancouver Island Range, about 150 km to the west of Vancouver (Fig. 1). A 21-m-
256 tall, 25-cm triangular open-lattice flux tower was erected in 2001 and equipped with
257 an EC system to continuously measure ~~turbulent fluxes of~~ H , LE , and F_{CO_2}
258 (Humphreys et al., 2006). In November 2017, this tower was decommissioned, and in
259 June 2017, a 33-m-tall walk-up scaffold flux tower (2 m wide x 4 m long) was erected
260 and equipped with an EC system to continuously measure H , LE , and F_{CO_2} . H , LE ,
261 and F_{CO_2} were calculated and F_{CO_2} was also corrected by adding the estimated rate of
262 change in CO_2 storage in the air column below the EC sensor height to obtain NEE
263 (Hollinger et al., 1994; Morgenstern et al., 2004). Fluxes during low turbulence
264 periods (~~friction velocity, u_*~~ , less than 0.16 m s^{-1}) were rejected (Lee et al., 2020a).
265 NEE was partitioned into GPP and R_e using a nighttime relationship model following
266 the Fluxnet-Canada Research Network procedure (Barr et al., 2004; Chen et al.,
267 2009). Four components of radiation were continuously measured by a CNR1 (Kipp
268 and Zonen) at the 32-m height facing south. α was calculated as ~~$K_{\downarrow}/K_{\uparrow}$~~ $K_{\uparrow}/K_{\downarrow}$ at noon
269 as done for the wetland site. PAR_g was measured using a quantum sensor (LI-190, LI-
270 COR Inc.) at the same height. Incoming diffuse PAR (PAR_d)~~The diffuse fraction of~~
271 ~~PAR~~ was measured at the 32-m height facing south (Sunshine sensor type BF3, Delta-
272 T Devices Ltd, Cambridge, UK). Information ~~of on the~~ quantum sensor is described in
273 the next section. Further details of the site are described in Jassal et al. (2009),
274 Krishnan et al. (2009), and Lee et al. (2020b).

275 2.3 Diffuse photosynthetically active radiation and light use efficiency

276 As mentioned above, it has been found that the dependence of GPP on the fraction of
277 diffuse PAR (called “~~DF~~diffuse fraction” hereafter) is ecosystem dependent. In this
278 study, we estimated the maximum GPP increase using the relationship between
279 ~~ecosystem light use efficiency~~ (LUE) and ~~diffuse fraction~~DF, as well as the
280 relationship between ~~total incoming~~ PAR and ~~diffuse fraction~~DF. First, cloudy
281 conditions increase ~~incident incoming~~ diffuse radiation but also decrease ~~K_d total~~
282 ~~radiation (direct plus diffuse)~~, which can counteract productivity increases due to
283 diffuse radiation alone (Alton, 2008; Letts et al., 2005; Oliphant et al., 2011). Cloudy
284 conditions also affect other meteorological drivers of photosynthesis such as vapor
285 pressure deficit (VPD) and surface temperature that regulate stomatal conductance
286 and can confound quantification of the photosynthetic response to ~~diffuse fraction~~DF
287 (Strada et al., 2015). In order to exclude this, we only included the day that was just
288 before or just after the study periods if it ~~was were~~ sunny. Extraterrestrial solar
289 radiation (K_{ext}), the flux density of solar radiation at the outer edge of atmosphere,
290 was also calculated using date, time, and latitude at the sites to obtain atmospheric
291 bulk transmissivity ($T = K_d/K_{ext}$), and hence determine whether a day was sunny
292 (~~defined as~~ $T > 0.65$).

293 Second, as there was no diffuse PAR measurement at the Burns Bog site, the
294 formula (~~DF~~diffuse fraction = $1.45 - 1.81T$) following Gu et al. (2002) and Alton
295 (2008) was used to estimate ~~DF~~the diffuse fraction for this site. Also, ~~DF~~diffuse
296 ~~fraction~~ was set at 0.95 when T was less than 0.28 and at 0.10 when T was greater
297 than 0.75. ~~DF~~The diffuse fraction at the Buckley Bay site in 2015 was estimated using
298 the same method because diffuse PAR measurement was not ~~yet~~ available ~~yet~~. For the
299 later three episodes, ~~DF~~the diffuse fraction was calculated as ~~the diffuse PAR~~ (PAR_d)
300 measured by the BF3 divided by ~~the incoming total PAR~~ (PAR_g) measured by the
301 quantum sensor.

302 Following Cheng et al. (2016), LUE ($\mu\text{mol CO}_2 (\mu\text{mol photon})^{-1}$) was defined as
303 the ratio of mean daily GPP ($\mu\text{mol m}^{-2} \text{s}^{-1}$) to mean daily PAR_g ($\mu\text{mol m}^{-2} \text{s}^{-1}$), which
304 gives $\text{GPP} = \text{LUE} \times \text{PAR}_g$. ~~One important note, LUE is defined as GPP per unit~~
305 ~~absorbed PAR_g (i.e. APAR = fAPAR x PAR_g), where fAPAR is the fraction of the~~
306 ~~absorbed PAR_g. Generally, fAPAR is affected by leaf area index (LAI), the solar~~
307 ~~zenith angle, and other factors such as leaf color (Ezhova et al., 2018). Typically,~~
308 ~~fAPAR for tree heights greater than 10 m and at a moderate zenith angle (i.e., 40–60°)~~
309 ~~can be estimated to be between 0.8 and 0.9 (Hovi et al., 2016). Besides DF, air~~
310 ~~temperature (T_a) and VPD are two additional environmental factors that can influence~~
311 ~~stomatal conductance and photosynthesis, and thus affect GPP (Cheng et al., 2015).~~
312 ~~To assess the impacts of changes in T_a and VPD on GPP in addition to diffuse~~

313 fraction, we first followed Cheng et al. (2015) to obtain GPP residuals (i.e., GPP
314 changes caused by factors other than direct PAR). The coefficients used in the
315 Michaelis–Menten light response function (rectangular hyperbola) were from Lee et
316 al. (2017) and Lee et al. (2020) for the wetland and forest sites, respectively. After
317 obtaining GPP residuals, we used Equation 3 and 4 in Cheng et al. (2015) to estimate
318 the proportions of variation in GPP residuals explained by DF, T_a , and VPD.
319

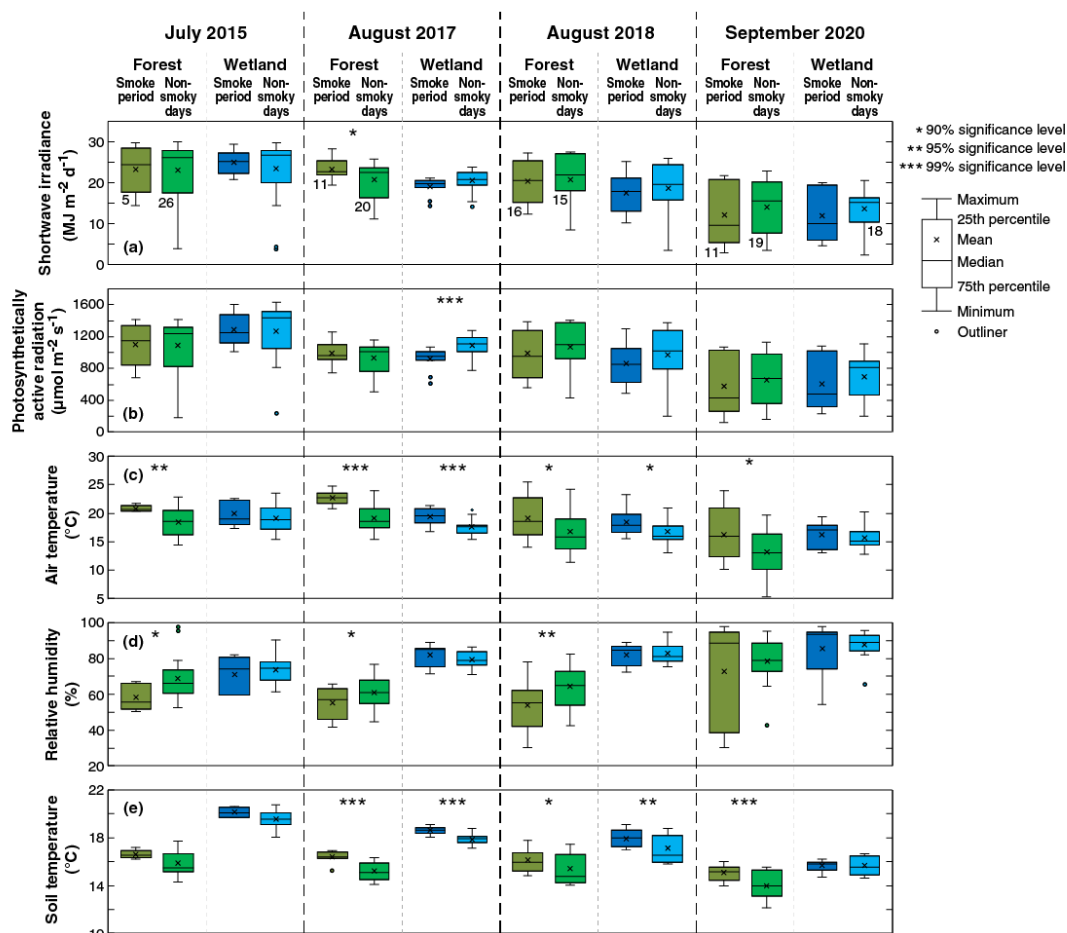
320 3 Results

321 3.1 Radiative changes and biophysical responses

322 3.1.1 Radiation and environmental conditions

323 Fig. 3 shows boxplots for measured K_l , PAR_g , ~~air temperature (T_a)~~, RH, and soil
324 temperature (T_s) during the smoky days (as defined in Table 1) and non-smoky days
325 (defined as all the remaining days in the same month) over the study periods. ~~The~~
326 ~~boxplot shows the mean, median, interquartile range, and outlier values.~~ Tests of
327 significance are also shown in Figs. 3 and 4 to indicate when differences between the
328 smoky and non-smoky days are statistically significant and at what significance level
329 (Students T tests). During days that were not affected by smoke, both sites
330 experienced a smooth diurnal course of radiation components consistent with typical
331 summer clear-sky conditions. Mean K_l values were generally lower during the
332 smoke events compared to the days that were not affected by smoke (Fig. 3), but these
333 differences were not statistically significant with the exception of the August 2017
334 event at ~~Burns Bog~~Buckley Bay. The difference was much greater for the September
335 2020 case. A few low K_l values were observed during those non-smoky days and
336 were likely due to the rain events (Fig. S1). On non-smoky days, mean daily T values
337 were approximately 70% at the two sites except during 2020 when it was ~60% (Fig.
338 4). The mean T values during the smoky days typically dropped to ~60% but
339 decreased to ~40% in 2020 (Fig. 4). In 2015, the most dramatic impact of the smoke
340 plume on K_l occurred on 5 July at Buckley Bay and 6 July at Burns Bog,
341 respectively, during otherwise clear sky conditions (Fig. S2). ~~The m~~Mean daily T
342 dropped to ~35% and ~50% at Buckley Bay and at Burns Bog, respectively (Fig. S3).
343 During the summer ~~in of~~ 2017, the wetland site experienced the biggest impact of
344 smoke on 4 August when T decreased to ~40% (Fig. S3). ~~One~~Two days later, on 6
345 August, the forest site was most affected by the smoke with T reduced to ~50% (Fig.
346 S3). The longest duration smoke episode of the four occurred in 2018, and reduced T
347 much earlier at Buckley Bay (11 August) than at Burns Bog (19 August). The
348 magnitudes of the decrease in T were similar at the two sites (dropped to ~35%) in
349 2018 (Fig. S3). The September 2020 case is notable for being the latest (season-wise)
350 of the four cases, and the only case in which K_l was reduced below 10 W m^{-2} at both
351 sites (Fig. S2). Mean daily T values in September were about 70% at the two sites
352 under sunny days (Fig. S3). T decreased appreciably to ~10% and 20% at Buckley
353 Bay and at Burns Bog, respectively, due to the smoke. These were the lowest values
354 among the four study periods. Both T_a and T_s were higher during the smoky days than
355 non-smoky days (Fig. 2), and the differences were ~~mostly generally~~ statistically
356 significant, ~~with~~ T_s ~~experienced experiencing~~ smaller changes compared to T_a . RH
357 dropped at the forest site during the smoke events except the 2020 case. In contrast,

358 the wetland site had higher RH when affected by wildfire smoke but the changes were
 359 not statistically significant. This partially reflects the substantial difference in wetness
 360 between the two sites.
 361



362
 363 **Figure 3.** Box plots of daily shortwave irradiance, average of total incoming
 364 photosynthetically active radiation during daytime, daily average of air temperature,
 365 daily average of relative humidity, and daily average of soil temperature during the
 366 smoke episodes and non-smoky days in that month over the study periods and other
 367 days, respectively, in 2015, 2017, 2018, and 2020 at Buckley Bay (the forest site) and
 368 at Burns Bog (the peatland site). The numbers of daily cases (n) used in the
 369 significance tests for each period for both the forest and wetland sites are shown
 370 beneath the boxplot pairs for the forest site in panel a. Unless otherwise shown, n is
 371 the same for all other variables and boxplot pairs in the same year.
 372

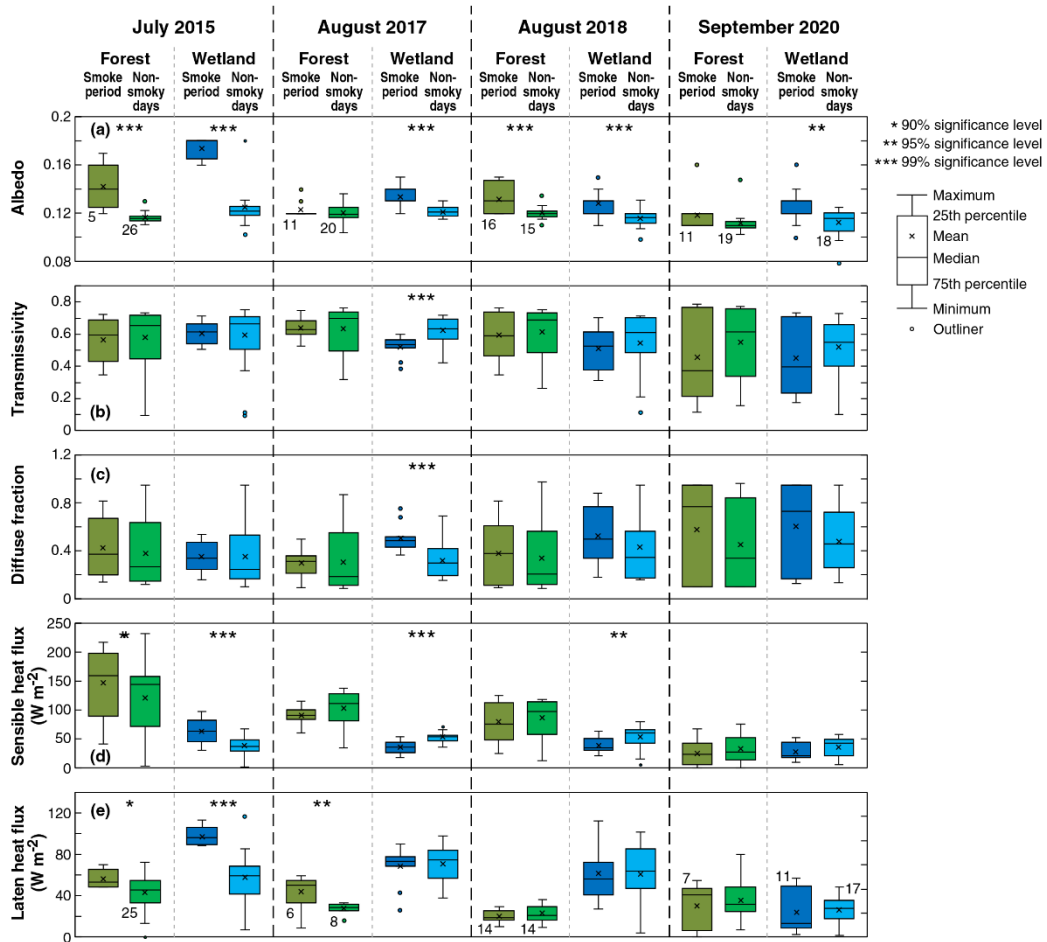
373 3.1.2 Albedo and energy partitioning

374 Under non-smoky conditions, mean albedo values were 0.12 and 0.13 at Buckley Bay
375 and Burns Bog, respectively (Fig. 4). These relatively low values are expected as the
376 forest site has taller vegetation that will trap light more effectively, while the wetland
377 site has dark water surfaces that lead to a lower albedo. A slight increase in albedo
378 was observed at both sites with the arrival of smoke during the four study periods and
379 the increases were mostly statistically significant. In 2015, the albedo increased more
380 than the other three years, especially at the wetland site. Excluding the 2015 case, the
381 increase in albedo was only ~ 10% at both sites.

382 The ~~differences changes~~ in H and LE ~~betweenduring~~ the smoky ~~and non-smoky~~
383 days were different every year ~~compared to the non-smoky days~~ (Fig. 4). Cloudy
384 conditions could play a role in determining magnitudes of H and LE . Thus, the mean
385 daytime ~~time~~-values of H and LE are also shown in Fig. ~~S3S4~~. As with K_d in 2015,
386 the most significant impact on H was on 5 July at Buckley Bay and Burns Bog, where
387 H decreased to 18% and 45% ~~respectively~~ of non-smoky mean daytime ($PAR_g \geq 20$
388 $\mu\text{mol m}^{-2} \text{s}^{-1}$) values. The impacts on LE were less than for H at both sites, with the
389 minimum for LE occurring on 9 July. At both sites, the Bowen ratio, β ($= H/LE$) was
390 appreciably reduced on 5 July, with the greater reduction at Buckley Bay (i.e., from
391 3.22 to 0.84) due to the large reduction in H . ~~In 2017, H during the smoky days was~~
392 ~~~85% of non-smoky mean daytime time value at the Buckley Bay site. However, LE~~
393 ~~increased significantly ($p < 0.05$) at Buckley Bay during the smoke period by ~60%~~
394 ~~of non-smoky mean daytime time values. During the 2018 smoke episode, Buckley~~
395 ~~Bay showed a similar decrease in H as 2017 but LE decreased slightly compared to~~
396 ~~2017. During the 2017 and 2018 smoke events, H at Burns Bog decreased to ~33%~~
397 ~~and ~27% of non-smoky mean daytime time values in 2017 and 2018, respectively,~~
398 ~~while LE remained similar as the non-smoky mean daytime time values. In September~~
399 ~~2020, the latest of the four smoke episodes, H and LE dropped to low values at both~~
400 ~~sites for the smoky and non-smoky days (Fig. S4)n 2017, the smallest decrease in H ,~~
401 ~~which maintained at 45% of non-smoky mean daytime time values, was found for~~
402 ~~Buckley Bay among the four study periods. However, LE dropped appreciably at~~
403 ~~Buckley Bay (14% of non-smoky mean daytime time values). During the 2018 smoke~~
404 ~~episode, Buckley Bay showed a similar response in H as 2015 but LE still decreased~~
405 ~~more than 2015. During 2017 and 2018 smoke events, H and LE had a similar~~
406 ~~response at Burns Bog. H decreased to 32% and 34% of non-smoky mean daytime~~
407 ~~time values in 2017 and 2018, respectively, while LE decreased to 27% and 34% of~~
408 ~~non-smoky mean daytime time values, respectively, but the differences in LE were~~
409 ~~not statistically significant. In September 2020, the latest of the four smoke episodes,~~

410 ~~*H* and *LE* dropped below 5 and 10 W m⁻² at Buckley Bay and Burns Bog,~~
411 ~~respectively.~~

412 In summary, the forest site had higher *H* than the wetland site during the smoky
413 days, except for the 2020 case (Fig. 4). Similarly, *LE* was consistently higher at the
414 wetter site (Burns Bog) compared to the forest site during smoky days, except for the
415 2020 case.~~In summary, the forest site had higher *H* than the wetland site during the~~
416 ~~smoky days, except for the 2020 case (Fig. 4). *LE* was maintained at a higher value at~~
417 ~~the wetter site (Burns Bog) compared to the forest site during smoke conditions.~~ Due
418 to the smaller changes in *H* and *LE*, β at Burns Bog stayed near 50% of non-smoky
419 mean daytime time values. However, β at Buckley Bay responded much more
420 dramatically and the observed range of β was between 26 and 90% of non-smoky
421 mean daytime ~~time~~ values. We also compared *H* and *LE* between smoky and sunny
422 days (Table S1). The results from the two comparisons (smoky vs. non-smoky days
423 and smoky vs. sunny days) mostly agreed with each other, although greater
424 differences were found when comparing smoky and sunny days.



426
 427
 428
 429
 430
 431
 432
 433
 434
 435

Figure 4. Box plots of noon-time albedo-at-noon, daytime daily average of transmissivity, daily average of diffuse fraction, daily average of sensible heat flux, and daily average of latent heat flux at the forest and wetland sites during the smoke events and non-smoky days, respectively, in 2015, 2017, 2018, and 2020. The numbers of daily cases (n) used in the significance tests for each period for both the forest and wetland sites are shown beneath the boxplot pairs for the forest site in panel a. Unless otherwise shown, n is the same for all other variables and boxplot pairs in the same year.

436 3.1.3 Diffuse radiation fraction

437 Fig. 4 shows ~~the diffuse fraction~~DF (mean daytime daily-PAR_d / mean daytime daily-
438 PAR_g) during the four smoke episodes at Buckley Bay. Under non-smoky conditions
439 over the four years, PAR_d is roughly a constant fraction of PAR_g (i.e., ≈ 0.30). With
440 the arrival of smoke in July or August, ~~the diffuse fraction~~DF increased to about 0.40.
441 When the smoke arrived later in the season, as in September 2020, DF increased
442 appreciably to almost 0.80. There was another peak in DF on 23 September 2020
443 daytime (Fig. S3).~~the diffuse fraction increased significantly to almost 0.80. There~~
444 ~~was another peak in diffuse fraction on 23 September 2020 (Fig. S3).~~ We attribute this
445 to intermittent transport events linked to the original smoke episode. Over the four
446 study periods, mean daily PAR_g values decreased during the smoke events (Fig. 3),
447 suggesting that during heavy smoke, scattering and absorption of incoming PAR_g was
448 enhanced.

449

450

451 3.2 Biogeochemical responses

452 3.2.1 Net ecosystem exchange

453 Daily totals for NEE are shown in Fig. 5. Both sites became a stronger CO₂ sink when
454 the smoke was present except in the September 2020 case. These increases were
455 statistically significant in the first two years with the exception of the July 2015 event
456 at Buckley Bay. The average change in daily (24-h) totals of NEE was about -1.00 g
457 C m⁻² day⁻¹ during the three years prior to 2020 with this increase in sink strength
458 primarily driven by an increase in GPP (Fig. 5). The increase in GPP (~ 2.00 g C m⁻²
459 day⁻¹) was generally more prominent than the decrease in R_e (< 1.00 g C m⁻² day⁻¹) ~~in~~
460 ~~general.~~ NEE during the September 2020 case did not change because both GPP and
461 R_e showed little response to the smoke.

462 Throughout the 2015 smoke period, Burns Bog remained a CO₂ sink and showed
463 an increasingly negative trend in NEE (stronger CO₂ sink) over the duration of the
464 smoke episode. Before the smoke arrived at the bog, the mean daily NEE was about -
465 1.60 g C m⁻² day⁻¹. The peak biogeochemical impact of the smoke at Burns Bog
466 occurred on 7 July, which led to a daily NEE of -3.64 g C m⁻² day⁻¹ (~~net~~-CO₂ sink)
467 (Fig. S5). Conversely, on 5 July, when the peak reduction of K_l was observed, NEE
468 at the forest site became more positive (a stronger CO₂ source~~a greater atmospheric~~
469 ~~source of CO₂~~). The Buckley Bay forest site became a strong ~~net~~-CO₂ sink on 6 and 7
470 July (-1.35 and -2.31 g C m⁻² day⁻¹, respectively) when the smoke had started to
471 disperse (Fig. S6).

472 In 2017, Burns Bog again became a stronger CO₂ sink (daily NEE < -2.5 g C m⁻²
473 day⁻¹) for three days (4–6 August) due to smoke (Fig. S5). The biogeochemical

474 impacts of smoke were somewhat different at Buckley Bay, where daily NEE showed
475 little change until the last day of the study period, when NEE decreased to -5.40 g C
476 $\text{m}^{-2} \text{ day}^{-1}$ (stronger CO_2 sink) on (Fig. S6). ~~The biogeochemical impacts of smoke were~~
477 a little different at Buckley Bay, where daily NEE showed little change until-
478 decreasing to $-5.40 \text{ g C m}^{-2} \text{ day}^{-1}$ (stronger CO_2 sink) on the last day of the study period
479 (Fig. S6).

480 During the 2018 episode, both ecosystems became a CO_2 sink for the three days
481 that smoke affected the sites (13 to 15 August at Burns Bog, and 11 to 13 August at
482 Buckley Bay) (Fig. S5 and S6). Both sites switched sites became a CO_2 sink for three
483 days that smoke affected Burns Bog on later dates (13 to 15 August) compared to-
484 Buckley Bay (11 to 13 August) (Fig. S5 and S6). Both sites changed from being CO_2
485 neutral to being a moderate CO_2 sink of about $-2.50 \text{ g C m}^{-2} \text{ day}^{-1}$.

486 Throughout the 2020 smoke period, when DFthe diffuse fraction was the highest
487 of all cases (0.30 to 0.80) appreciable significant impacts on NEE were observed at
488 both sites. Buckley Bay and Burns Bog bBoth became stronger CO_2 sinks between 11
489 and 12 September (going from -0.57 to $-4.00 \text{ g C m}^{-2} \text{ day}^{-1}$ and from -0.40 to -1.40 g
490 $\text{C m}^{-2} \text{ day}^{-1}$, respectively) (Fig. S5 and S6). However, after PAR_g dropped to low
491 values, both sites turned into weak CO_2 sources (2.10 and $0.37 \text{ g C m}^{-2} \text{ day}^{-1}$ for
492 Buckley Bay and Burns Bog, respectively).

493 As was done for *H* and *LE*, we compared daily averages of NEE during smoky
494 and sunny days (Table S1). Large differences between smoky and sunny days were
495 also found in this case.

497 3.2.2 Gross primary production and ecosystem respiration

498 Measured NEE was partitioned into GPP and R_e to further investigate the
499 biogeochemical responses of the two sites to smoke (Fig. 5). In general, most of the
500 differences changes in GPP and R_e between the smoky and non-smoky during the
501 smoke periods compared to the non-smoky days were statistically significant.
502 In the 2015 smoke event at Buckley Bay, daily GPP increased about $2 \text{ g C m}^{-2} \text{ day}^{-1}$
503 while daily R_e increased by only about $1.5 \text{ g C m}^{-2} \text{ day}^{-1}$, which resulted in the site
504 becoming a slightly stronger CO_2 sink. At Burns Bog, the responses were somewhat
505 different with the relative increase in daily GPP by $\sim 1.5 \text{ g C m}^{-2} \text{ day}^{-1}$ and decrease in
506 daily R_e by $\sim 0.2 \text{ g C m}^{-2} \text{ day}^{-1}$.

507 Due to missing data, an appreciable increase in CO_2 sequestration was observed
508 on only one day (6 August) at Buckley Bay in 2017 (Fig. S6). This was
509 predominantly controlled by the sizeable increase in daily GPP (170%), while the
510 increase in daily R_e was minimal at 40%. The increase in daily GPP also played a role
511 in increasing CO_2 sequestration at Burns Bog; however, the increase in GPP was not

512 as great as at Buckley Bay. At Burns Bog the increase in daily GPP was about 20%
513 while the decrease in daily R_e was 25%.

514 Compared to the previous two years where both sites became stronger CO₂ sinks
515 from being weak CO₂ sinks, the changes in 2018 at the two sites were similar but
516 slightly smaller. The main reason was the weaker increase in daily GPP. The Burns
517 Bog site had about a 30% higher daily GPP during the smoke event than during non-
518 smoky conditions (Fig. S5). However, the Buckley Bay site experienced about the
519 same mean daily GPP during the smoke event ($3.1 \text{ g C m}^{-2} \text{ day}^{-1}$) as during non-
520 smoky conditions ($3.0 \text{ g C m}^{-2} \text{ day}^{-1}$).

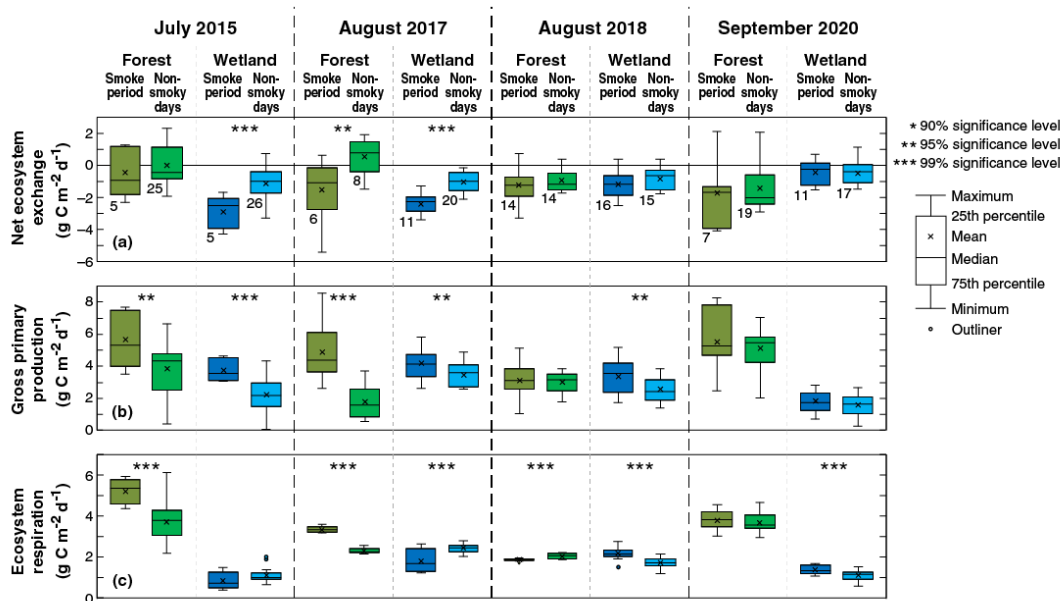
521 Throughout the 2020 smoke event, there were small increases in daily GPP of about
522 ~10% at both sites. Due to the heavy smoke permitting only low PAR_g on 13
523 September, daily GPP dropped rapidly by about 70% compared to the previous days
524 (Fig. S5 and S6), which resulted in the two sites switching from being CO₂ sinks to
525 CO₂ sources over the course of one day. In the 2015 smoke event at Buckley Bay,
526 daily GPP increased about 25% while daily R_e decreased by only about 5%, which
527 resulted in the site becoming a CO₂ sink. At Burns Bog, the responses were somewhat
528 different than those at Buckley Bay. Here, the relative increase in daily GPP and
529 decrease in daily R_e were similar with both being ~60%.

530 Due to missing data, the increase in CO₂ sequestration was only appreciable on one
531 day (6 August) at Buckley Bay in 2017 (Fig. S6). This was predominantly controlled
532 by the sizeable increase in daily GPP (140%), while the decrease in daily R_e was
533 minimal at 4%. The increase in daily GPP also played a role in increasing CO₂-
534 sequestration at Burns Bog but it was not as strong as at Buckley Bay, where the
535 increases in daily GPP were about 30% and the decreases in daily R_e were smaller at
536 15%.

537 Compared to the previous two years where both sites became stronger CO₂ sinks from
538 being weak CO₂ sinks, the changes in 2018 at the two sites were similar but slightly
539 smaller. The main factor was the weaker rise in daily GPP. The Burns Bog wetland-
540 site had about 30% higher daily GPP during the smoke event than during non-smoky-
541 conditions (Fig. S5). But the Buckley Bay forest site experienced about the same daily
542 GPP during the smoke event as during non-smoky conditions (Fig. S6).

543 Throughout the 2020 smoke event, there were marked increases in daily GPP of about
544 90% at both sites. Due to the heavy smoke permitting only low PAR_g on 13-
545 September, daily GPP rapidly dropped by about 70% compared to the previous days-
546 (Fig. S5 and S6). This resulted in the two sites switching from CO₂ sinks to sources-
547 over one day.

548



549

550 **Figure 5.** Box plots of net ecosystem exchange (NEE), gross primary production
 551 (GPP), and ecosystem respiration (R_e) at the forest site during the smoke events and
 552 non-smoky days, respectively, in 2015, 2017, 2018, and 2020. The numbers of daily
 553 cases (n) used in the significance tests for each period for both the forest and wetland
 554 sites are shown beneath the boxplot pairs for the forest site in panel a. Unless
 555 otherwise shown, n is the same for all other variables and boxplot pairs in the same
 556 year.

557

558

559 3.2.3 Relationship between smoke and gross primary production

560 Fig. 6a shows the dependence of mean PAR_g on ~~DF~~the diffuse fraction for the two
 561 sites. As expected, PAR_g decreases linearly as ~~DF~~the fraction increases ($R^2 = 0.86$ and
 562 0.80 for Buckley Bay and Burns Bog, respectively). PAR_g decreased ~10% more
 563 rapidly (~~~10%~~) at the wetland site than the forest site. The relationship between LUE
 564 and ~~the diffuse fraction~~ DF was also examined in order to better understand the
 565 behaviour of the dependence of GPP on ~~DF~~the diffuse fraction (Fig. 6b). A linear
 566 relationship is evident with an R^2 ~~at of~~ 0.52 and 0.34 for Buckley Bay and Burns Bog,
 567 respectively. LUE at the forest site increased with increasing DF by a factor of ~3
 568 more than at the wetland site. ~~LUE at the forest site increased much more when the~~
 569 ~~diffuse fraction increased, which was ~2 times more than at the wetland site.~~

570

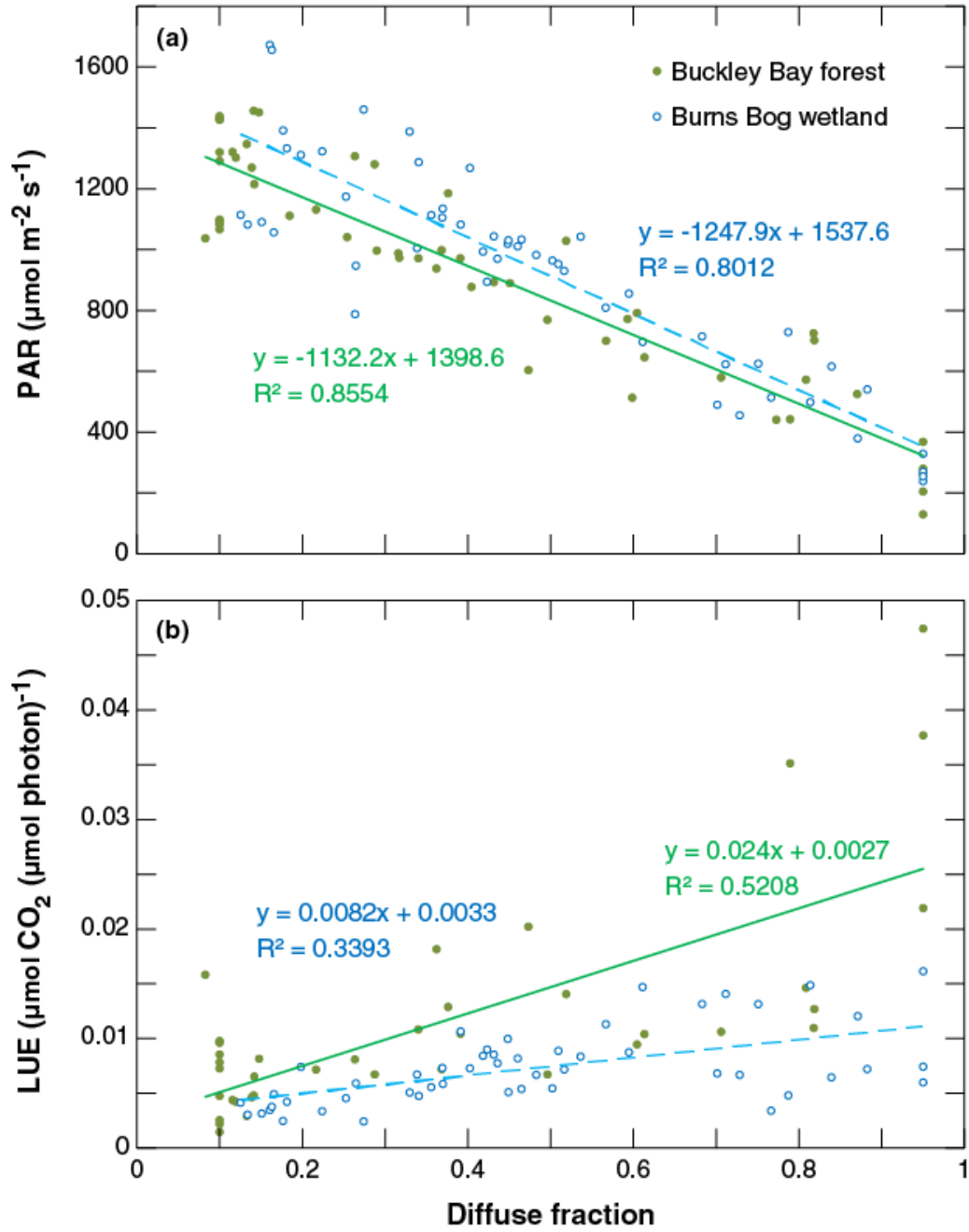
571

572

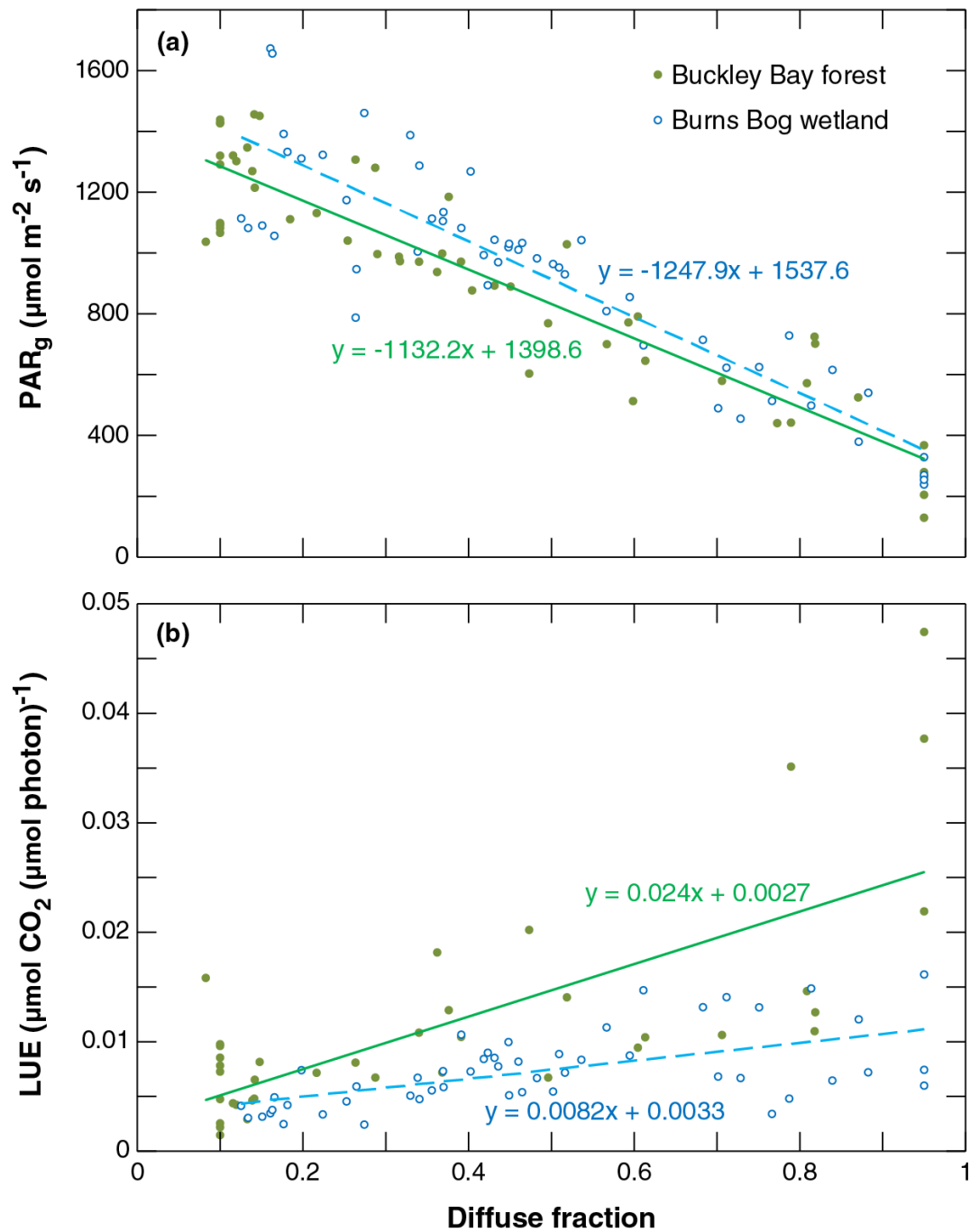
573

By conducting the simple and multiple linear regressions, we investigated the
amount of variance in GPP residuals attributable to the three environmental variables
(i.e., DF , T_a and VPD). When including the effects of T_a and VPD on GPP residuals
with DF , the amount of variation in GPP residuals explained increased by up to an

574 additional 38% (at the forest site) with an average of 24% and 9% at the forest and
575 wetland sites, respectively (Table S2). A combination of three variables explained
576 more than 90% of the variation in GPP residuals when the smoke arrived earlier in
577 summer (i.e., July 2017) for both sites and for the forest site in August 2018. The only
578 case for which T_a and VPD explained more of the variation in GPP residuals than DF
579 was at the forest site during August 2017, which was the same month that the site
580 experienced the greatest drop in LE .
581



582



583

584 **Figure 6.** (a) Total incoming photosynthetically active radiation (PAR_g) as a function
 585 of the diffuse fraction of PAR_g (DF). (b) Light use efficiency (LUE) as a function of
 586 the diffuse fraction of PAR_g DF.

587 4 Discussion

588 4.1 Impact of smoke episodes on radiation and biophysical properties

589 Over the four study years, significant perturbation of both the radiation and energy
590 budgets over the forest and wetland ecosystems in southwestern BC was observed
591 when a dense layer of wildfire smoke impacted the region. Generally, changes were
592 more pronounced at the Buckley Bay forest site on Vancouver Island relative to the
593 Burns Bog wetland site in Metro Vancouver.

594 The observed decreases in K_{\downarrow} at the two sites during the four study periods were
595 minimal when comparing smoky and non-smoky days. In order to compare to other
596 studies, we also compared K_{\downarrow} between smoky and sunny days (Table 2), as was done
597 for H , LE , and NEE . The average decreases in K_{\downarrow} at both sites were about the same
598 at $\sim 20\%$. ~~The observed decreases in K_{\downarrow} at the two sites during the four study periods~~
599 were about 50% and 40% for the forest and wetland sites, respectively. These values
600 are comparable (~~Table 2~~) with to reported reductions ~~of total solar irradiance in K_{\downarrow}~~ by
601 forest fire smoke in Brazil (the Brazilian Amazon with AOD_{500} peaking at 3.0) and
602 Africa (Zambian savanna with AOD_{500} peaking at 2.0) (Schafer et al., 2002). Similar
603 agreement is also apparent when compared with the 2010 fires in central Russia that
604 led to a reduction of K_{\downarrow} of about 40% (Chubarova et al., 2012) or 80 W m^{-2} (Péré et
605 al., 2014) and the 2017 Chilean mega-fires, which resulted in a decrease in that made
606 K_{\downarrow} drop of about 100 W m^{-2} (Lapere et al., 2021). The reduction of in K_{\downarrow} reported by
607 from Rosário et al. (2013) was smaller at about 55 W m^{-2} when AOD_{500} was near 2.0
608 during the 2002 biomass burning season in ~~south~~ South America. Although the
609 AOD_{550} value was slightly lower than in this study, Yamasoe et al. (2017) reported
610 that K_{\downarrow} was reduced by about 50 W m^{-2} over the spring, during the period of long
611 range transport of biomass burning plumes, in São Paulo, Brazil. In our study, we
612 found that K_{\downarrow} dropped to near ~~0-3 and $5 \text{ MJ m}^{-2} \text{ day}^{-1} \text{ W m}^{-2}$ and that lower values~~
613 were about 90% and 70% of non-smoky conditions at the forest and wetland sites,
614 respectively, during the smoke episode in September 2020. ~~The~~ This reduction was
615 much greater than the previous three smoke episodes (Figure S2).

616 As with K_{\downarrow} , turbulent heat fluxes (H and LE) were appreciably affected by
617 smoke at the two sites with a greater impact at the Buckley Bay forest site. These
618 results are consistent in both direction and magnitude with previous studies elsewhere
619 where the reduction in K_{\downarrow} due to aerosols in turn impacted H and LE (Feingold et al.,
620 2005; Jiang and Feingold, 2006; Mallet et al., 2009; Markowicz et al., 2021; Steiner et
621 al., 2013). It is important to note that these results were similar despite the cited
622 locations study sites being in ~~quite different~~ geographical settings quite different
623 from than in this study. Furthermore, they were associated with significantly lower
624 AOD_{550} values than observed in the four BC smoke episodes.

625 It is important to note that energy partitioning can be very different in different
626 ecosystems (Steiner et al., 2013). As discussed above, H was reduced significantly in
627 2017, 2018 and 2020 at the Buckley Bay forest site where canopy effects are most
628 important. The possible mechanism could be that the switch from high direct radiation
629 to predominately diffuse radiation during the smoke episodes likely caused the
630 reduction in H as a consequence of reduced heating of leaves in a highly coupled
631 forest canopy (Brümmer et al., 2012). In this study, the wetland site offers an
632 interesting contrast to the Buckley Bay forest site. As McKendry et al. (2019) noted,
633 with standing water as a result of restoration at the wetland site, and little
634 physiological control on LE , the impacts on the energy partitioning were modest
635 compared to the physiologically controlled LE at Buckley Bay. Another factor
636 affecting energy partitioning is accessibility to soil moisture. Our results indicate that
637 LE at the forest site increased in 2015 and 2017 and remained about the same in 2018
638 during the smoke periods. This might be because the trees were still able to maintain
639 transpiration by using water from deeper soil layers. Soil moisture also plays a role at
640 the wetland site. Generally, the wetland site also had higher LE than H during the
641 smoke episodes except in September 2020. This was likely because water level
642 dropped below the rooting depth of most bog vegetation (Lee et al., 2017). For both H
643 and LE , when the smoke arrived at the later stage of summer (September 2020),
644 impacts were the smallest of the four study periods. This is likely because both sites
645 had the lowest available energy during this period and were dry after two months of
646 low precipitation. Another factor affecting energy partitioning is soil moisture. Our
647 results indicate that LE at the forest site dropped much more in 2017 and 2018 than
648 2015. This might be due to generally drier soil conditions in August than in July,
649 especially the extreme dry summer during which there was only 1 mm of precipitation
650 in July and August 2017 (Lee et al., 2020b). Soil moisture also plays a role at the
651 wetland site. Generally, the site also had higher LE than H during the smoke episodes
652 except in September 2020. This was likely because water level dropped below the
653 rooting depth of most bog vegetation (Lee et al., 2017). For both H and LE , when the
654 smoke arrived at the later stage of summer (September 2020), impacts were the
655 greatest of the four study periods. This was attributed to the fact that both sites were
656 dry after two months of low precipitation.

657 Only a slight increase in albedo was observed at both sites with the arrival of
658 smoke during the four study periods. This was probably likely due to reduction in
659 specular reflection during direct solar irradiance and an increase in diffuse reflection.
660 However, Nojarov et al. (2021) found that the albedo of the underlying surface greatly
661 affects the radiative effect of aerosols at Musala (altitude is 2925 m), Bulgaria. The
662 results indicated that aerosol amount, at surface level, has had a negative radiative

663 effect when albedo values ~~are-were~~ low (< 0.4) but a positive radiative effect when
664 albedo values ~~are-were~~ high (> 0.4). They explained that higher albedo can lead to
665 larger amounts of reflected and scattered shortwave radiation, especially close to the
666 earth's surface. At higher aerosol amounts the result is an increase in ~~the amount of~~
667 scattered shortwave radiation, which also increases the global solar radiation.

668 **Table 2.** Observed decreased shortwave irradiance (K_d) during the study smoke
 669 periods and several estimates from previously published studies.
 670

Event	AOD value	Decrease in K_d	Reference
2015, BC	AOD ₅₀₀ = ~4.5	52% or 180 W m ⁻²	Buckley Bay site
	AOD ₅₀₀ = ~3.0	30% or 104 W m ⁻²	Burns Bog site
2017, BC	AOD ₅₀₀ = ~1.5	31% or 101 W m ⁻²	Buckley Bay site
	AOD ₅₀₀ = ~2.5	37% or 98 W m ⁻²	Burns Bog site
2018, BC	AOD ₅₀₀ = ~3.5	50% or 157 W m ⁻²	Buckley Bay site
		47% or 120 W m ⁻²	Burns Bog site
2020, BC	AOD ₅₀₀ not available	87% or 231 W m ⁻²	Buckley Bay site
		69% or 120 W m ⁻²	Burns Bog site
1999, Brazil	AOD ₅₀₀ = 0.5~3.0	9~37%	Schafer et al. (2002)
2000, Africa	AOD ₅₀₀ = 0.5~2.0	13~37%	Schafer et al. (2002)
2010, central Russia	AOD ₅₀₀ = 2.5	40%	Chubarova et al. (2012)
2002, South America	AOD ₅₀₀ = 0.2~2.0	10~55 W m ⁻²	Rosário et al. (2013)
2010, Central Russia	AOD ₃₄₀ = 2.0~4.0	70~84 W m ⁻²	Péré et al. (2014)
2005~2015, Brazil	AOD ₅₅₀ = 0.6~1.0	50 W m ⁻²	Yamasoe et al. (2017)
2017, Chile	AOD ₅₅₀ = 4.0	100 W m ⁻²	Lapere et al. (2021)

671

672 4.2 Effects of aerosol loading on biogeochemical properties

673 The typical ~~diffuse fraction~~DF in southwestern BC under sunny conditions ($T > 0.65$)
674 over these four years was ~ 0.1530 . Generally, when ~~the diffuse fraction~~DF increased
675 to between 0.40 and 0.50 due to wildfire smoke, the two sites became a stronger CO₂
676 sink (i.e., NEE became more negative). However, these responses were also
677 controlled by ~~other factors, such as~~VPD and T_{sa} . When PAR_g dropped to low values,
678 even if ~~PAR_a fraction~~DF exceeded 0.80, ~~the both~~ study ~~forest and wetland ecosystems~~
679 ~~both sites~~ became a CO₂ source_s. These broad patterns are comparable to previous
680 research in different environments (Niyogi et al., 2004; Park et al., 2018; Yamasoe et
681 al., 2006). An observational study in the Amazon rainforest found that, under
682 moderate AOD₅₀₀, CO₂ uptake was enhanced by the increased ~~DF~~diffuse fraction
683 (Yamasoe et al., 2006). Park et al. (2018) also indicated that moderate levels of smoke
684 resulted in small increases in CO₂ sequestration, while extremely smoky conditions
685 resulted in lower CO₂ sequestration as the effect of the reduction in PAR_g outweighed
686 the DRF effect.

687 The changes in NEE were primarily controlled by changes in GPP (Fig. 5).
688 Therefore, in this study, we further investigated how GPP responded to smoke using
689 the relationship between PAR_g and ~~DF~~diffuse fraction, as well as the relationship
690 between LUE and ~~DF~~diffuse fraction. Ezhova et al. (2018) analyzed data from five
691 forest sites that included two mixed forests and three Scots pine (*Pinus sylvestris* L.)
692 forests (55-, 60-, and 100-year old). In that region, ~~DF~~diffuse fraction was
693 approximately 0.11 on days characterized by low aerosol loading and about 0.25 on
694 days with moderate aerosol loading. They also found that PAR_g decreased as
695 ~~DF~~diffuse fraction increased at across the five sites. Compared ~~toing~~ their ~~estimated~~
696 ~~coefficients (values of~~ PAR_g at zero ~~DF~~diffuse fraction), the Buckley Bay forest and
697 Burns Bog wetland sites had values (1399 and 1538 $\mu\text{mol m}^{-2} \text{s}^{-1}$, respectively)
698 similar to those of four of the five forests (1480 to about 1608 $\mu\text{mol m}^{-2} \text{s}^{-1}$). PAR_g
699 under clear-sky conditions was much lower at the 60-year old Scots pine site
700 (SMEAR I, 1212 $\mu\text{mol m}^{-2} \text{s}^{-1}$) compared with the other sites, which was partly due to
701 its high latitude (Ezhova et al., 2018). Generally, the slopes of the linear dependences
702 in the relationship between PAR_g and DF were similar in this study, which can likely
703 be attributed to similar cloud attenuating properties (Ezhova et al., 2018). ~~site had a~~
704 ~~similar value (~~ $-1132 \mu\text{mol m}^{-2} \text{s}^{-1}$) ~~to the 100-year old Scots pine forest (~~ $-1118 \mu\text{mol}$
705 ~~$\text{m}^{-2} \text{s}^{-1}$).~~ The Burns Bog wetland site had a slightly higher coefficient ($-1248 \mu\text{mol m}^{-2}$
706 s^{-1}) among all these sites ($-944 \mu\text{mol m}^{-2} \text{s}^{-1}$ to about $-1194 \mu\text{mol m}^{-2} \text{s}^{-1}$). Generally,
707 ~~the slopes of the linear dependences in the relationship of PAR_g and diffuse fraction~~
708 ~~were similar, which can likely be attributed to similar cloud attenuating properties~~
709 ~~(Ezhova et al., 2018).~~

710 The slope in the relationship ~~of betwee~~ LUE and ~~diffuse fraction~~DF reflects
711 canopy properties such as leaf area index and thickness of canopy (Ezhova et al.
712 2018). The Buckley Bay forest site had a slope of $0.0240 \mu\text{mol CO}_2 (\mu\text{mol photon})^{-1}$,
713 which is about three times higher than the value ~~found at for~~ the Burns Bog wetland
714 site ($0.0082 \mu\text{mol CO}_2 (\mu\text{mol photon})^{-1}$). This indicates the ability of a forest stand to
715 take up more CO₂ in response to an increasing ~~diffuse fraction of PAR~~DF. Ezhova et
716 al. (2018) found that two mixed forest sites (0.0238 to $0.0278 \mu\text{mol CO}_2 (\mu\text{mol}$
717 $\text{photon})^{-1}$) had steeper LUE slopes compared to the other three coniferous forest sites
718 (about $0.015 \mu\text{mol CO}_2 (\mu\text{mol photon})^{-1}$ ~~o~~n average). They attributed the difference
719 to mixed forests having a larger potential for photosynthetic activity enhancement due
720 to a larger leaf area index and a deeper canopy. Results from mixed and broadleaf
721 forest sites in the USA showed the increase in LUE was about $0.03 \mu\text{mol CO}_2 (\mu\text{mol}$
722 $\text{photon})^{-1}$ (Cheng et al., 2016). Hemes et al. (2020) analyzed the EC measurements
723 across one corn (C4 plant), one alfalfa (C3 plant), and two restored wetland (C3
724 plants) sites during ~~the a~~ summer 2018 smoke event in California, USA. The slope of
725 the relationship between LUE and ~~diffuse fraction~~DF for the corn site ($0.0190 \mu\text{mol}$
726 $\text{CO}_2 (\mu\text{mol photon})^{-1}$) was intermediate between the mature alfalfa site ($0.0270 \mu\text{mol}$
727 $\text{CO}_2 (\mu\text{mol photon})^{-1}$) and the two restored wetland sites (0.0140 and $0.0180 \mu\text{mol}$
728 $\text{CO}_2 (\mu\text{mol photon})^{-1}$). This indicates that corn is more sensitive than the wetlands but
729 less sensitive than alfalfa. Their restored wetland ecosystems ~~are were~~ both
730 characterized by quasi-managed mixes of tule and cattail vegetation with
731 aboveground water ~~tables~~levels. Thus, these two sites had lower LUE sensitivities to
732 ~~diffuse fraction~~DF compared to the two crop sites. Our wetland site has even shorter
733 vegetation compared to theirs and thus an even lower sensitivity (~40% lower).

734 Finally, based on the linear dependence of LUE on ~~diffuse fraction~~DF and PAR_g
735 on ~~diffuse fraction~~DF, we estimated how GPP changed with ~~diffuse fraction~~DF. An
736 increase up to ~7% in GPP was found at the Burns Bog wetland site. GPP at the
737 Buckley Bay forest site ~~can~~increased by up to ~18%, which is slightly higher than
738 the consistent with results from Ezhova et al. (2018) showing an increase in GPP
739 between 6% and 14% at five forest sites. Increases of 3–4.1% and 1.6–2.4% in GPP
740 due to a 1% increase in DF were found for tree species and non-tree species,
741 respectively, using 200 FLUXNET sites by Zhou et al. (2021). Hemes et al. (2020)
742 found that the GPP enhancement was between 0.71%, and 1.16% at four sites for
743 every 1% increase in ~~diffuse fraction~~DF when absorbed PAR_g was held constant. Lee
744 et al. (2018) also showed a comparable GPP enhancement at 0.94% GPP using a
745 process-based sun-shade canopy model with observations from a broadleaf forest in
746 the eastern USA.

747 ~~Our results also indicated that other environmental drivers that co-varied with~~
748 ~~DF can contribute to explaining GPP residuals under wildfire smoke events.~~
749 ~~Generally, T_a and VPD appeared to have small effects on GPP residuals at the two~~
750 ~~study sites (Table S2). In only one of the study events (Buckley Bay in 2017) did T_a~~
751 ~~and VPD account for more variation in GPP residuals than DF itself. Cheng et al.~~
752 ~~(2015) also observed this for mixed conifer forests, which implies radiation changes~~
753 ~~can have a less important role when T_a and VPD can greatly increase stomatal~~
754 ~~conductance under smoky conditions at conifer forests.~~ We note that although the
755 empirical models based on conditional sampling in this study are able to explain much
756 of the variation in observations, they have limitations compared to more mechanistic,
757 process-based models (Knobl and Baldocchi, 2008; Lee et al., 2018). On the other
758 hand, process-based models often require parameterizations for specific vegetation
759 and photosynthetic types that introduce more complexities and hence probably lead to
760 higher uncertainty (Hemes et al., 2020).

762 4.3 Study limitations

763 Due to their limited spatial and temporal scale, the results described here have
764 limitations that restrict attempts to generalise (and easily scale up). Firstly, although
765 the four cases examined extend our understanding of biophysical and biogeochemical
766 impacts to a wider range of cases than McKendry et al. (2020), they are by no means
767 exhaustive, nor are they likely representative of the broad variety of forest types
768 across BC.

769 Secondly, attribution of ecosystem responses wholly to smoke, while rigorously
770 controlling for other environmental variables (e.g., air quality, antecedent moisture
771 conditions, wind, cloudiness, RH, temperature) is challenging. Our ~~rudimentary-~~
772 ~~simple~~ tests of significance highlight that whilst there is a clear signal of biophysical
773 and biogeochemical responses to smoke, it is by no means consistent across all four
774 events, each land-use type, or all variables. This suggests that each smoke event is
775 somewhat unique in terms of antecedent conditions, present weather conditions and
776 the characteristics of the smoke itself (e.g., age, elevation, composition, density). For
777 example, in addition to the effects of ~~diffuse fraction~~DF, wildfire smoke often
778 incorporates a complex mixture of gases (e.g., CO, CH₄, NO_x, and O₃), aerosols, and
779 aerosol precursors (Crutzen et al., 1979; Jaffe and Wigder, 2012; Pfister et al., 2008).
780 ~~Increased-Although increased~~ O₃ and co-pollutants are often associated with wildfires
781 (Jaffe & Wigder, 2012; Pfister et al., 2008; Yamasoe et al., 2006) and can have an
782 indirect impact on ~~the~~ecosystem carbon budgets that is harder to quantify (Malavelle
783 et al., 2019). ~~None of these effects are addressed in this study.~~We did not observe an
784 ~~appreciable increase in hourly ozone maxima, nor daily average O₃ during the four~~

785 smoke episodes (Table 1). Maximum hourly values at both sites were generally below
786 60 ppb while daily average values during smoke events were within 2-3 ppb of overall
787 monthly average values. On this basis and using the results of Hemes et. al. (2020),
788 we estimated that O₃ enhancements in smoke would contribute to a ~ 1% GPP
789 reduction at Buckley Bay and Burns Bog.

790 An important note is that LUE is usually defined as GPP per unit absorbed PAR_g
791 (i.e. APAR = fAPAR x PAR_g), where fAPAR is the fraction of the absorbed PAR_g.
792 Generally, fAPAR is affected by leaf area index (LAI), the solar zenith angle, and
793 other factors such as leaf color (Ezhova et al., 2018). Due to the temporal and spatial
794 variation in these factors we chose to base the definition on PAR_g. Typically, fAPAR
795 for tree heights greater than 10 m and at a moderate zenith angle (i.e., 40–60°) can be
796 estimated to be between 0.8 and 0.9 (Hovi et al., 2016).

797 Finally, we have compared smoky and non-smoky conditions exclusively during
798 the months of these events. This is somewhat arbitrary and ~~by default necessarily~~
799 neglects a wide range of meteorological variability associated with each “type”.

800 However, this ~~rudimentary-simple~~ approach serves to highlight the complex
801 combination of processes involved. Various combinations of cloudiness, antecedent
802 meteorological conditions, wind, etc. all control biophysical and biogeochemical
803 responses, with smoke being only one of the factors at play. Isolating the individual
804 impact of smoke is challenging. There are, however, common elements that can be
805 gleaned from this inter-comparison of four cases. In particular, the presence of
806 wildfire smoke is shown to have a statistically significant impact on ~~diffuse-~~
807 ~~radiation~~DF that has the potential to turn both natural and managed ecosystems into a
808 carbon sink when smoke densities are low to moderate. In this sense, this work is
809 consistent with both theory and observations elsewhere and confirms that wildfire
810 smoke ~~likely has can have~~ a significant impact on regional carbon budgets.

811 5 Conclusions

812 Aerosol loading from wildfire smoke is not only becoming a regular component of air
813 quality considerations in a warming world, but has climate impacts and unexplored
814 feedbacks. Through biogeochemical and biophysical processes, wildfire smoke
815 influences the climate by altering both greenhouse gas dynamics and how energy and
816 water are exchanged between the ecosystem and the atmosphere. Clearly, under
817 conditions in which the presence of wildfire smoke is more frequent, and perhaps of
818 longer duration, the results described herein imply substantial impacts on the regional
819 energy and carbon budgets.

820

821 Results from four major smoke events in different years are broadly consistent with
822 those described elsewhere. Specifically for the forest and wetland ~~two~~ sites examined;

- 823 • The maximum reduction in daily totals of K_d due to smoke was generally about
824 50% but reached 90% in the September 2020 case and was near 100% in dense
825 smoke.
- 826 • During smoky days, the forest site had higher H than the wetland site and the
827 wetland site had higher LE than the forest site during the smoky days. However,
828 when the smoke arrived later (e.g., September 2020), both sites had similar H
829 and LE in smoky conditions. This was attributed to the markedly reduced K_d
830 and to both sites being dry after two months of low precipitation.
- 831 • Under non-smoky conditions during the summer months, DF in southwestern
832 British Columbia is ~ 0.30 . The presence of smoke generally increased it to
833 ~ 0.50 with dense smoke increasing values to ~ 0.95 . When total
834 photosynthetically active radiation dropped to low values, however, both the
835 forest and wetland ecosystems turned into net CO_2 sources.
- 836 • Based on our estimates, GPP can increase by up to $\sim 18\%$ and $\sim 7\%$ at the forest
837 and wetland sites, respectively, due to the direct effect of smoke particles
838 compared to clean atmospheric conditions.
- 839 • ~~The reduction in incoming solar radiation due to smoke was generally about~~
840 ~~50% but reached 90% in the September 2020 case and was near 100% in dense~~
841 ~~smoke.~~
- 842 • ~~The forest site had a more dramatic change in the ratio of sensible heat to latent~~
843 ~~heat flux (i.e., the Bowen ratio). When the smoke arrived later (e.g., September~~
844 ~~2020), impacts on turbulent heat fluxes were the greatest for both sites. This was~~
845 ~~attributed to the markedly reduced incoming solar radiation and to both sites~~
846 ~~being dry after two months of low precipitation.~~
- 847 • ~~Under non-smoky conditions during the summer months, diffuse fraction in~~
848 ~~southwestern British Columbia is ~ 0.30 . The presence of smoke generally~~

849 ~~increased it to ~0.50 with dense smoke increasing values to ~0.95. When total~~
850 ~~photosynthetically active radiation dropped to low values, however, both the~~
851 ~~forest and wetland ecosystems turned into CO₂ sources.~~
852 • ~~Photosynthesis can be increased by ~18% and ~7% due to the direct effect of~~
853 ~~smoke particles compared to clean conditions in the forest and wetland sites,~~
854 ~~respectively.~~

855

856 This study confirms a clear signal of diffuse radiation fertilization across four major
857 smoke episodes, resulting in forest and wetland becoming enhanced carbon sinks
858 under ~~some-most~~ smoke conditions, with the exception of heavy smoke conditions.
859 This has implications for the regional carbon budget if the duration and frequency of
860 smoke events increases as a result of climate change. However, we identify significant
861 limitations in this preliminary research and identify a complex array of processes that
862 contribute to biophysical and biogeochemical responses. Before attempting to scale
863 up, further research is required in different forest types across the region and to
864 identify and control for the numerous myriad processes and feedbacks influencing
865 local carbon budgets in forest and wetland ecosystems.

866 **6 Acknowledgements**

867 We are grateful to the Natural Sciences and Engineering Research Council of Canada
868 (NSERC) for support to individual researchers and graduate students involved in this
869 work. The Buckley Bay flux tower was funded by ~~the~~ NSERC and ~~The~~ the Canadian
870 Foundation for Innovation (CFI). We sincerely thank Island Timberlands LP for the
871 permission to work on their land and their logistical support. The Burns Bog flux
872 tower operation was funded by Metro Vancouver through contracts to Drs. Andreas
873 Christen and Sara Knox. Selected instrumentation was supported by NSERC and CFI.
874 We ~~thans~~ the substantial technical and logistical support by ~~staffs~~ from Metro
875 Vancouver and the City of Delta. We greatly appreciate the assistance of Robert
876 Halsall, Rick Ketler, Zoran Nestic, and Marion Nyberg with their invaluable field and
877 technical support.

878 **7 References**

- 879 Alton, P., Mercado, L. and North, P.: A sensitivity analysis of the land-surface scheme
880 JULES conducted for three forest biomes: Biophysical parameters, model processes,
881 and meteorological driving data, *Global Biogeochem. Cycles*, 20(1), 2006.
- 882 Alton, P. B.: Reduced carbon sequestration in terrestrial ecosystems under overcast
883 skies compared to clear skies, *Agric. For. Meteorol.*, 148(10), 1641–1653, 2008.
- 884 Barr, A. G., Black, T. A., Hogg, E. H., Kljun, N., Morgenstern, K. and Nesic, Z.: Inter-
885 annual variability in the leaf area index of a boreal aspen-hazelnut forest in relation to
886 net ecosystem production, *Agric. For. Meteorol.*, 126(3–4), 237–255, 2004.
- 887 Brümmer, C., Black, T. A., Jassal, R. S., Grant, N. J., Spittlehouse, D. L., Chen, B.,
888 Nesic, Z., Amiro, B. D., Arain, M. A. and Barr, A. G.: How climate and vegetation
889 type influence evapotranspiration and water use efficiency in Canadian forest,
890 peatland and grassland ecosystems, *Agric. For. Meteorol.*, 153, 14–30, 2012.
- 891 Chen, B., Black, T. A., Coops, N. C., Hilker, T., Trofymow, J. A. T. and Morgenstern,
892 K.: Assessing tower flux footprint climatology and scaling between remotely sensed
893 and eddy covariance measurements, *Boundary-Layer Meteorol.*, 130(2), 137–167,
894 2009.
- 895 Cheng, S. J., Bohrer, G., Steiner, A. L., Hollinger, D. Y., Suyker, A., Phillips, R. P.
896 and Nadelhoffer, K. J.: Variations in the influence of diffuse light on gross primary
897 productivity in temperate ecosystems, *Agric. For. Meteorol.*, 201, 98–110, 2015.
- 898 Cheng, S. J., Steiner, A. L., Hollinger, D. Y., Bohrer, G. and Nadelhoffer, K. J.: Using
899 satellite-derived optical thickness to assess the influence of clouds on terrestrial
900 carbon uptake, *J. Geophys. Res. Biogeosciences*, 121(7), 1747–1761, 2016.
- 901 Christen, A., Jassal, R. S., Black, T. A., Grant, N. J., Hawthorne, I., Johnson, M. S.,
902 Lee, S.-C. and Merckens, M.: Summertime greenhouse gas fluxes from an urban bog
903 undergoing restoration through rewetting., *Mires Peat*, 17, 2016.
- 904 Chubarova, N., Nezval, Y., Sviridenkov, I., Smirnov, A. and Slutsker, I.: Smoke
905 aerosol and its radiative effects during extreme fire event over Central Russia in
906 summer 2010, *Atmos. Meas. Tech.*, 5(3), 557, 2012.
- 907 Crutzen, P. J. and Andreae, M. O.: Biomass burning in the tropics: Impact on
908 atmospheric chemistry and biogeochemical cycles, *Science (80-.)*, 250(4988), 1669–
909 1678, 1990.
- 910 Crutzen, P. J., Heidt, L. E., Krasnec, J. P., Pollock, W. H. and Seiler, W.: Biomass
911 burning as a source of atmospheric gases CO, H₂, N₂O, NO, CH₃Cl and COS,
912 *Nature*, 282(5736), 253–256, 1979.
- 913 D’Acunha, B., Morillas, L., Black, T. A., Christen, A. and Johnson, M. S.: Net
914 ecosystem carbon balance of a peat bog undergoing restoration: integrating CO₂ and

915 CH₄ fluxes from eddy covariance and aquatic evasion with DOC drainage fluxes, J.
916 Geophys. Res. Biogeosciences, 124(4), 884–901, 2019.

917 Doughty, C. E., Flanner, M. G. andGoulden, M. L.: Effect of smoke on subcanopy
918 shaded light, canopy temperature, and carbon dioxide uptake in an Amazon rainforest,
919 Global Biogeochem. Cycles, 24(3), 2010.

920 Ezhova, E., Ylivinkka, I., Kuusk, J., Komsaare, K., Vana, M., Krasnova, A., Noe, S.,
921 Arshinov, M., Belan, B. andPark, S.-B.: Direct effect of aerosols on solar radiation
922 and gross primary production in boreal and hemiboreal forests, Atmos. Chem. Phys.,
923 2018.

924 Feingold, G., Jiang, H. andHarrington, J. Y.: On smoke suppression of clouds in
925 Amazonia, Geophys. Res. Lett., 32(2), 2005.

926 Ferrara, M., Pomeroy, C., McKendry, I. G., Stull, R. andStrawbridge, K.: Suppression
927 of “Handover” Processes in a Mountain Convective Boundary Layer due to Persistent
928 Wildfire Smoke, Boundary-Layer Meteorol., 1–12, 2020.

929 Gu, L., Baldocchi, D., Verma, S. B., Black, T. A., Vesala, T., Falge, E. M. andDowty,
930 P. R.: Advantages of diffuse radiation for terrestrial ecosystem productivity, J.
931 Geophys. Res. Atmos., 107(D6), ACL-2, 2002.

932 Hemes, K. S., Verfaillie, J. andBaldocchi, D. D.: Wildfire-smoke aerosols lead to
933 increased light use efficiency among agricultural and restored wetland land uses in
934 California’s Central Valley, J. Geophys. Res. Biogeosciences, 125(2),
935 e2019JG005380, 2020.

936 Hollinger, D. Y., Kelliher, F. M., Byers, J. N., Hunt, J. E., McSeveny, T. M. andWeir,
937 P. L.: Carbon dioxide exchange between an undisturbed old-growth temperate forest
938 and the atmosphere, Ecology, 75(1), 134–150, 1994.

939 Hovi, A., Liang, J., Korhonen, L., Kobayashi, H. andRautiainen, M.: Quantifying the
940 missing link between forest albedo and productivity in the boreal zone,
941 Biogeosciences, 13(21), 6015–6030, 2016.

942 Humphreys, E. R., Black, T. A., Morgenstern, K., Cai, T., Drewitt, G. B., Nesic, Z.
943 andTrofymow, J. A.: Carbon dioxide fluxes in coastal Douglas-fir stands at different
944 stages of development after clearcut harvesting, Agric. For. Meteorol., 140(1–4), 6–
945 22, 2006.

946 Jacobson, M. Z.: Effects of biomass burning on climate, accounting for heat and
947 moisture fluxes, black and brown carbon, and cloud absorption effects, J. Geophys.
948 Res. Atmos., 119(14), 8980–9002, 2014.

949 Jaffe, D. A. andWigder, N. L.: Ozone production from wildfires: A critical review,
950 Atmos. Environ., 51, 1–10, 2012.

951 Jassal, R. S., Black, T. A., Spittlehouse, D. L., Brümmer, C. andNesic, Z.:
952 Evapotranspiration and water use efficiency in different-aged Pacific Northwest
953 Douglas-fir stands, *Agric. For. Meteorol.*, 149(6–7), 1168–1178, 2009.

954 Jiang, H. andFeingold, G.: Effect of aerosol on warm convective clouds: Aerosol-
955 cloud-surface flux feedbacks in a new coupled large eddy model, *J. Geophys. Res.*
956 *Atmos.*, 111(D1), 2006.

957 Kanniah, K. D., Beringer, J., North, P. andHutley, L.: Control of atmospheric particles
958 on diffuse radiation and terrestrial plant productivity: A review, *Prog. Phys. Geogr.*,
959 36(2), 209–237, 2012.

960 Knohl, A. andBaldocchi, D. D.: Effects of diffuse radiation on canopy gas exchange
961 processes in a forest ecosystem, *J. Geophys. Res. Biogeosciences*, 113(G2), 2008.

962 Krishnan, P., Black, T. A., Jassal, R. S., Chen, B. andNesic, Z.: Interannual variability
963 of the carbon balance of three different-aged Douglas-fir stands in the Pacific
964 Northwest, *J. Geophys. Res. Biogeosciences*, 114(G4), 2009.

965 Landry, J.-S., Matthews, H. D. andRamankutty, N.: A global assessment of the carbon
966 cycle and temperature responses to major changes in future fire regime, *Clim.*
967 *Change*, 133(2), 179–192, 2015.

968 Lapere, R., Mailler, S. andMenut, L.: The 2017 Mega-Fires in Central Chile: Impacts
969 on Regional Atmospheric Composition and Meteorology Assessed from Satellite Data
970 and Chemistry-Transport Modeling, *Atmosphere (Basel)*., 12(3), 344, 2021.

971 Lasslop, G., Coppola, A. I., Voulgarakis, A., Yue, C. andVeraverbeke, S.: Influence
972 of fire on the carbon cycle and climate, *Curr. Clim. Chang. Reports*, 5(2), 112–123,
973 2019.

974 Lee, M. S., Hollinger, D. Y., Keenan, T. F., Ouimette, A. P., Ollinger, S.V
975 andRichardson, A. D.: Model-based analysis of the impact of diffuse radiation on
976 CO₂ exchange in a temperate deciduous forest, *Agric. For. Meteorol.*, 249, 377–389,
977 2018.

978 Lee, S.-C., Black, T. A., Jassal, R. S., Christen, A., Meyer, G. andNesic, Z.: Long-
979 term impact of nitrogen fertilization on carbon and water fluxes in a Douglas-fir stand
980 in the Pacific Northwest, *For. Ecol. Manage.*, 455, 117645, 2020a.

981 Lee, S.-C., Christen, A., Black, T. A., Jassal, R. S., Ketler, R. andNesic, Z.:
982 Partitioning of net ecosystem exchange into photosynthesis and respiration using
983 continuous stable isotope measurements in a Pacific Northwest Douglas-fir forest
984 ecosystem, *Agric. For. Meteorol.*, 292, 108109, 2020b.

985 Lee, S. C., Christen, A., Black, A. T., Johnson, M. S., Jassal, R. S., Ketler, R., Nesic,
986 Z. andMerkens, M.: Annual greenhouse gas budget for a bog ecosystem undergoing
987 restoration by rewetting, *Biogeosciences*, 14(11), 2799–2814, 2017.

988 Letts, M. G., Lafleur, P. M. and Roulet, N. T.: On the relationship between cloudiness
989 and net ecosystem carbon dioxide exchange in a peatland ecosystem, *Ecoscience*,
990 12(1), 53–69, 2005.

991 Malavelle, F. F., Haywood, J. M., Mercado, L. M., Folberth, G. A., Bellouin, N.,
992 Sitch, S. and Artaxo, P.: Studying the impact of biomass burning aerosol radiative and
993 climate effects on the Amazon rainforest productivity with an Earth system model,
994 *Atmos. Chem. Phys.*, 19(2), 1301–1326, 2019.

995 Mallet, M., Tulet, P., Serça, D., Solmon, F., Dubovik, O., Pelon, J., Pont, V.
996 and Thouron, O.: Impact of dust aerosols on the radiative budget, surface heat fluxes,
997 heating rate profiles and convective activity over West Africa during March 2006,
998 *Atmos. Chem. Phys.*, 9(18), 7143–7160, 2009.

999 Markowicz, K. M., Lisok, J. and Xian, P.: Simulations of the effect of intensive
1000 biomass burning in July 2015 on Arctic radiative budget, *Atmos. Environ.*, 171, 248–
1001 260, 2017.

1002 Markowicz, K. M., Zawadzka-Manko, O., Lisok, J., Chilinski, M. T. and Xian, P.: The
1003 impact of moderately absorbing aerosol on surface sensible, latent, and net radiative
1004 fluxes during the summer of 2015 in Central Europe, *J. Aerosol Sci.*, 151, 105627,
1005 2021.

1006 McKendry, I., Strawbridge, K., Karumudi, M. L., O’Neill, N., Macdonald, A. M.,
1007 Leitch, R., Jaffe, D., Cottle, P., Sharma, S. and Sheridan, P.: Californian forest fire
1008 plumes over Southwestern British Columbia: lidar, sunphotometry, and mountaintop
1009 chemistry observations, *Atmos. Chem. Phys.*, 11(2), 465–477, 2011.

1010 McKendry, I. G., Christen, A., Sung-Ching, L., Ferrara, M., Strawbridge, K. B.,
1011 O’Neill, N. and Black, A.: Impacts of an intense wildfire smoke episode on surface
1012 radiation, energy and carbon fluxes in southwestern British Columbia, Canada,
1013 *Atmos. Chem. Phys.*, 19(2), 835–846, 2019.

1014 Millennium Ecosystem Assessment: Ecosystems and human well-being, Island press
1015 United States of America., 2005.

1016 Ministry of Forests: British Columbia’s forests: and their management. [online]
1017 Available from: <https://www.for.gov.bc.ca/hfd/pubs/Docs/Mr/Mr113.htm>, 2003.

1018 Ministry of Forests Mines and Land: The State of British Columbia’s Forests Third
1019 Edition. [online] Available from:
1020 [https://www2.gov.bc.ca/assets/gov/environment/research-monitoring-and-](https://www2.gov.bc.ca/assets/gov/environment/research-monitoring-and-reporting/reporting/envreportbc/archived-reports/sof_2010.pdf)
1021 [reporting/reporting/envreportbc/archived-reports/sof_2010.pdf](https://www2.gov.bc.ca/assets/gov/environment/research-monitoring-and-reporting/reporting/envreportbc/archived-reports/sof_2010.pdf), 2010.

1022 Moncrieff, J. B., Massheder, J. M., DeBruin, H., Elbers, J., Friborg, T., Heusinkveld,
1023 B., Kabat, P., Scott, S., Søgaard, H. and Verhoef, A.: A system to measure surface
1024 fluxes of momentum, sensible heat, water vapour and carbon dioxide, *J. Hydrol.*, 188,
1025 589–611, 1997.

1026 Moreira, D. S., Longo, K. M., Freitas, S. R., Yamasoe, M. A., Mercado, L. M.,
1027 Rosário, N. E., Gloor, E., Viana, R. S. M., Miller, J. B. and Gatti, L. V.: Modeling the
1028 radiative effects of biomass burning aerosols on carbon fluxes in the Amazon region,
1029 2017.

1030 Morgenstern, K., Black, T. A., Humphreys, E. R., Griffis, T. J., Drewitt, G. B., Cai,
1031 T., Nesic, Z., Spittlehouse, D. L. and Livingston, N. J.: Sensitivity and uncertainty of
1032 the carbon balance of a Pacific Northwest Douglas-fir forest during an El Niño/La
1033 Niña cycle, *Agric. For. Meteorol.*, 123(3–4), 201–219, 2004.

1034 Niyogi, D., Chang, H., Saxena, V. K., Holt, T., Alapaty, K., Booker, F., Chen, F.,
1035 Davis, K. J., Holben, B. and Matsui, T.: Direct observations of the effects of aerosol
1036 loading on net ecosystem CO₂ exchanges over different landscapes, *Geophys. Res.*
1037 *Lett.*, 31(20), 2004.

1038 Nojarov, P., Arsov, T., Kalapov, I. and Angelov, H.: Aerosol direct effects on global
1039 solar shortwave irradiance at high mountainous station Musala, Bulgaria, *Atmos.*
1040 *Environ.*, 244, 117944, 2021.

1041 Oliphant, A. J., Dragoni, D., Deng, B., Grimmond, C. S. B., Schmid, H.-P. and Scott,
1042 S. L.: The role of sky conditions on gross primary production in a mixed deciduous
1043 forest, *Agric. For. Meteorol.*, 151(7), 781–791, 2011.

1044 Oris, F., Asselin, H., Ali, A. A., Finsinger, W. and Bergeron, Y.: Effect of increased
1045 fire activity on global warming in the boreal forest, *Environ. Rev.*, 22(3), 206–219,
1046 2014.

1047 Pachauri, R. K., Allen, M. R., Barros, V. R., Broome, J., Cramer, W., Christ, R.,
1048 Church, J. A., Clarke, L., Dahe, Q. and Dasgupta, P.: Climate change 2014: synthesis
1049 report. Contribution of Working Groups I, II and III to the fifth assessment report of
1050 the Intergovernmental Panel on Climate Change, *Ipcc.*, 2014.

1051 Papale, D., Reichstein, M., Aubinet, M., Canfora, E., Bernhofer, C., Kutsch, W.,
1052 Longdoz, B., Rambal, S., Valentini, R. and Vesala, T.: Towards a standardized
1053 processing of Net Ecosystem Exchange measured with eddy covariance technique:
1054 algorithms and uncertainty estimation, *Biogeosciences*, 3(4), 571–583, 2006.

1055 Park, S.-B., Knohl, A., Lucas-Moffat, A. M., Migliavacca, M., Gerbig, C., Vesala, T.,
1056 Peltola, O., Mammarella, I., Kolle, O. and Lavrič, J. V.: Strong radiative effect
1057 induced by clouds and smoke on forest net ecosystem productivity in central Siberia,
1058 *Agric. For. Meteorol.*, 250, 376–387, 2018.

1059 Péré, J. C., Bessagnet, B., Mallet, M., Waquet, F., Chiapello, I., Minvielle, F., Pont,
1060 V. and Menut, L.: Direct radiative effect of the Russian wildfires and its impact on air
1061 temperature and atmospheric dynamics during August 2010, *Atmos. Chem. Phys.*,
1062 14(4), 1999–2013, 2014.

1063 Pfister, G. G., Wiedinmyer, C. and Emmons, L. K.: Impacts of the fall 2007 California
1064 wildfires on surface ozone: Integrating local observations with global model
1065 simulations, *Geophys. Res. Lett.*, 35(19), 2008.

1066 R Core Team: R: A language and environment for statistical computing, [online]
1067 Available from: <https://www.r-project.org/>, 2017.

1068 Rap, A., Spracklen, D.V., Mercado, L., Reddington, C. L., Haywood, J. M., Ellis, R.
1069 J., Phillips, O. L., Artaxo, P., Bonal, D. and Restrepo Coupe, N.: Fires increase
1070 Amazon forest productivity through increases in diffuse radiation, *Geophys. Res.*
1071 *Lett.*, 42(11), 4654–4662, 2015.

1072 Reichstein, M., Falge, E., Baldocchi, D., Papale, D., Aubinet, M., Berbigier, P.,
1073 Bernhofer, C., Buchmann, N., Gilmanov, T. and Granier, A.: On the separation of net
1074 ecosystem exchange into assimilation and ecosystem respiration: review and
1075 improved algorithm, *Glob. Chang. Biol.*, 11(9), 1424–1439, 2005.

1076 Rosário, N. E. do, Longo, K. M., Freitas, S. R. de, Yamasoe, M. A. and Fonseca, R.
1077 M. da: Modeling the South American regional smoke plume: aerosol optical depth
1078 variability and surface shortwave flux perturbation, *Atmos. Chem. Phys.*, 13(6),
1079 2923–2938, 2013.

1080 Schafer, J. S., Eck, T. F., Holben, B. N., Artaxo, P., Yamasoe, M. A. and Procopio, A.
1081 S.: Observed reductions of total solar irradiance by biomass-burning aerosols in the
1082 Brazilian Amazon and Zambian Savanna, *Geophys. Res. Lett.*, 29(17), 1–4, 2002.

1083 Sena, E. T., Artaxo, P. and Correia, A. L.: Spatial variability of the direct radiative
1084 forcing of biomass burning aerosols and the effects of land use change in Amazonia.,
1085 *Atmos. Chem. Phys.*, 13(3), 2013.

1086 Settele, J., Scholes, R., Betts, R. A., Bunn, S., Leadley, P., Nepstad, D., Overpeck, J.,
1087 Taboada, M. A., Fischlin, A. and Moreno, J. M.: Terrestrial and inland water systems,
1088 in *Climate change 2014 impacts, adaptation and vulnerability: Part A: Global and*
1089 *sectoral aspects*, pp. 271–360, Cambridge University Press., 2015.

1090 Steiner, A. L., Mermelstein, D., Cheng, S. J., Twine, T. E. and Oliphant, A.: Observed
1091 impact of atmospheric aerosols on the surface energy budget, *Earth Interact.*, 17(14),
1092 1–22, 2013.

1093 Strada, S., Unger, N. and Yue, X.: Observed aerosol-induced radiative effect on plant
1094 productivity in the eastern United States, *Atmos. Environ.*, 122, 463–476, 2015.

1095 Taubman, B. F., Marufu, L. T., Vant-Hull, B. L., Piety, C. A., Doddridge, B. G.,
1096 Dickerson, R. R. and Li, Z.: Smoke over haze: Aircraft observations of chemical and
1097 optical properties and the effects on heating rates and stability, *J. Geophys. Res.*
1098 *Atmos.*, 109(D2), 2004.

1099 Ward, D. S., Kloster, S., Mahowald, N. M., Rogers, B. M., Randerson, J. T. and Hess,
1100 P. G.: The changing radiative forcing of fires: global model estimates for past, present
1101 and future, *Atmos. Chem. Phys.*, 12(22), 10857–10886, 2012.

1102 Wetland Stewardship Partnership: Wetland Ways: Interim Guidelines for Wetland
1103 Protection and Conservation in British Columbia. [online] Available from:
1104 [https://www2.gov.bc.ca/gov/content/environment/air-land-water/water/water-](https://www2.gov.bc.ca/gov/content/environment/air-land-water/water/water-planning-strategies/wetlands-in-bc#:~:text=British Columbia%27s wetlands currently comprise,fish%2C birds and other wildlife., 2009)
1105 [planning-strategies/wetlands-in-bc#:~:text=British Columbia%27s wetlands currently](https://www2.gov.bc.ca/gov/content/environment/air-land-water/water/water-planning-strategies/wetlands-in-bc#:~:text=British Columbia%27s wetlands currently comprise,fish%2C birds and other wildlife., 2009)
1106 [comprise,fish%2C birds and other wildlife.](https://www2.gov.bc.ca/gov/content/environment/air-land-water/water/water-planning-strategies/wetlands-in-bc#:~:text=British Columbia%27s wetlands currently comprise,fish%2C birds and other wildlife., 2009), 2009.

1107 Wutzler, T., Lucas-Moffat, A., Migliavacca, M., Knauer, J., Sickel, K., Šigut, L.,
1108 Menzer, O. and Reichstein, M.: Basic and extensible post-processing of eddy
1109 covariance flux data with REddyProc, *Biogeosciences*, 15(16), 5015–5030, 2018.

1110 Yamasoe, M. A., Randow, C. von, Manzi, A. O., Schafer, J. S., Eck, T. F. and Holben,
1111 B. N.: Effect of smoke and clouds on the transmissivity of photosynthetically active
1112 radiation inside the canopy, *Atmos. Chem. Phys.*, 6(6), 1645–1656, 2006.

1113 Yamasoe, M. A., DoRosário, N. M. E. and Barros, K. M. de: Downward solar global
1114 irradiance at the surface in São Paulo city—The climatological effects of aerosol and
1115 clouds, *J. Geophys. Res. Atmos.*, 122(1), 391–404, 2017.

1116 Yu, H., Liu, S. C. and Dickinson, R. E.: Radiative effects of aerosols on the evolution
1117 of the atmospheric boundary layer, *J. Geophys. Res. Atmos.*, 107(D12), AAC-3,
1118 2002.

1119 Zhou, H., Yue, X., Lei, Y., Zhang, T., Tian, C., Ma, Y. and Cao, Y.: Responses of
1120 gross primary productivity to diffuse radiation at global FLUXNET sites, *Atmos.*
1121 *Environ.*, 244, 117905, 2021.

1122